

UNIVERSITÀ DEGLI STUDI DI NAPOLI "FEDERICO II"



SCUOLA DI MEDICINA E CHIRURGIA

Dipartimento di Neuroscienze, Scienze Riproduttive ed Odontostomatologiche

DOTTORATO IN NEUROSCIENZE – XXXI CICLO

Coordinatore: *Prof. Maurizio Tagliatela*

TESI DI DOTTORATO IN NEUROSCIENZE

Post mortem and in vivo study of multiple sclerosis pathogenesis

RELATORE

Prof.

Vincenzo Brescia Morra

CANDIDATO

Dott.

Marcello Moccia

ANNO ACCADEMICO 2017-2018

*To my dad and to my sister,
a family source of scientific rigour*

LIST OF ABBREVIATIONS

APC:	antigen-presenting cell
CNS:	central nervous system
CoQ10:	coenzyme Q10
CSF:	cerebrospinal fluid
CSV:	comma-separated values
DMT:	disease modifying treatment
DTI:	diffusion tensor imaging
EAE:	experimental autoimmune encephalomyelitis
EDSS:	expanded disability status scale
fMRI:	functional magnetic resonance imaging
GM:	grey matter
IFN:	interferon-gamma
IL:	interleukin
MT:	magnetization transfer
MTR:	magnetization transfer ratio
MRI:	magnetic resonance imaging
MRS:	magnetic resonance spectroscopy
MS:	multiple sclerosis
NA:	normal-appearing
ROI:	region of interest
TNF:	tumor necrosis factor
WM:	white matter

Post mortem and in vivo study of multiple sclerosis pathogenesis

TABLE OF CONTENTS

1. Abstract	p.	5
2. State of the art	p.	8
3. Objectives	p.	17
4. Defining the pathology of multiple sclerosis with latent-profile models		
4.1 Introduction	p.	18
4.2 Methods	p.	19
4.3 Results	p.	25
4.4 Discussion	p.	29
5. Pathological correlates of magnetization transfer ratio in multiple sclerosis		
5.1 Introduction	p.	34
5.2 Methods	p.	35
5.3 Results	p.	41
5.4 Discussion	p.	48
6. Peripheral markers of oxidative stress and inflammation in multiple sclerosis		
6.1 Introduction	p.	52
6.2 Methods	p.	53
6.3 Results	p.	61
6.4 Discussion	p.	73
7. Conclusions and future perspectives	p.	78
8. Acknowledgements	p.	80
9. References	p.	82

1. Abstract

Multiple Sclerosis (MS) is a chronic inflammatory disease of the central nervous system. A number of pathological mechanisms could be responsible for acute demyelination and chronic tissue remodelling in MS, including inflammation, oxidative stress, microglia activation, and astrocyte infiltrates. In the present work, we aim to further explore the heterogeneity of MS pathogenesis on *post mortem* brains, and to evaluate the possibility to study MS pathogenesis by using magnetic resonance imaging (MRI) and peripheral blood biomarkers.

In the first part of the study, we applied a data driven approach to classify MS patients in relation to the variety of pathological changes occurring in lesional and normal-appearing (NA) white matter (WM) and grey matter (GM), with subsequent clinical correlates. Tissue blocks from 16 MS brains were immunostained and quantified for neuro-axonal structures (NF200), myelin (SMI94), macrophages (CD68), B-lymphocytes (CD20), T-lymphocytes (CD3), cytotoxic T-lymphocytes (CD8), microglia (IBA1), astrocytes (GFAP), and mitochondrial damage. After semi-automatic registration of digitized histologic sections, regions-of-interest (ROIs) were manually defined in lesion and NA WM and GM. A latent class analysis was employed to characterize pathology subtypes in MS; different goodness of fit parameters (AIC, BIC, and G^2 statistics) were used to identify the number of classes that better characterize the MS sub-populations. Profile 1 (active remodelling) was characterized by normal-appearing neuro-axonal structures and intact energetic metabolism, with high levels of macrophages/microglia and astrocytes. Profile 2 (mitochondrial dysfunction) was characterized by severely impaired mitochondrial function, along with demyelination and neuroaxonal loss, and ongoing inflammatory changes, mainly driven by cytotoxic T-cells (CD8+); patients in profile 2 presented with more severe symptoms at onset and faster disability accrual, when compared with other profiles. Profile 3 (inactive) was characterized by severe demyelination

and axonal loss, with similarly reduced mitochondrial function, without any concomitant pathological process contributing to further tissue remodelling and/or damage. The possibility to classify each patient depending on his/her prevalent pathology profile support the concept of MS immunopathological homogeneity within the same patient and heterogeneity between different patients, and could be used to better profile MS patients and individualize their treatment.

In the second part of the study, we explored *post mortem* pathology-MRI correlates and specifically focused on an advanced MRI technique (magnetization transfer ratio -MTR-), ideally detecting myelin content. MTR is widely used in MS observational studies and clinical trials, but its pathological correlates remain unclear. MTR maps were acquired at 3 Tesla from sixteen fixed MS brains and four healthy controls. 101 tissue blocks were immunostained and quantified, as previously described. After semi-automatic registration of digitized histologic sections and MTR maps, ROIs were manually defined. Associations between MTR and each stain were explored using linear mixed regression models (with cassettes nested within patients); differences in the associations between ROIs were explored using interaction terms. Lower MTR was associated with lower levels of NF200, SMI94, CD68, IBA1 and GFAP, with higher levels of CD8 and greater mitochondrial damage; MTR was more strongly associated with SMI94 in GM than WM. In a multivariate linear mixed regression model including all ROIs and brains, SMI94 was the best correlate of MTR. Myelin immunostain intensity is the strongest correlate of MTR, especially when measured in the GM. However, the additional histological correlates of MTR have to be kept in mind when interpreting the results of MTR clinical studies and designing experimental trials in MS.

Finally, we evaluated the possibility to study (and to modify) MS pathology *in vivo*, by using biomarkers in the peripheral blood. Considering that oxidative stress is a driver of MS pathology, we evaluated the effect of coenzyme Q10 (CoQ10) on laboratory markers of oxidative stress and

inflammation, and on MS clinical severity, and, then, calculated the sample size needed to detect significant variations to define most promising biomarkers. We included 60 relapsing-remitting MS patients treated with Interferon-Beta1a-44 μ g with CoQ10 for 3 months, and with Interferon-Beta1a-44 μ g alone for 3 more months (open-label cross-over design). At baseline, 3- and 6-month visits, we measured markers of scavenging activity, oxidative damage and inflammation in the peripheral blood, and collected data on disease severity. After 3 months, CoQ10 supplementation was associated with improved scavenging activity (as mediated by uric acid), reduced intracellular reactive oxygen species production, reduced oxidative DNA damage, and shift towards a more anti-inflammatory milieu in the peripheral blood (with higher IL-4 and IL-13, and lower Eotaxin, GM-CSF, HGF, IFN- γ , IL-1 α , IL-2R, IL-9, IL-17F, MIP-1 α , RANTES, TNF- α and VEGF). Also, CoQ10 supplementation was associated with lower expanded disability status scale, fatigue severity scale, Beck's depression inventory, and visual analogic scale for pain. For sample size estimates, we used adjusted-beta-coefficients of observed 3-month variation for each laboratory measure (and respective standard deviation); we assumed that the observed variation was the highest achievable treatment effect (100%), and we estimated sample size for conservative treatment effects (e.g., 70%), smaller than what observed. Setting 5% alpha-error and 80% power, low sample size requirements to detect 70% observed variation from a baseline pre-treatment timepoint to a 3-month follow-up were found for IL-3 (n=1), IL-5 (n=1), IL-7 (n=4), IL-2R (n=4), IL-13 (n=6), IL-6 (n=14), IL-8 (n=22), IL-4 (n=23), RANTES (n=25), TNF- α (n=26), IL-1 β (n=27), and uric acid (n=29). CoQ10 supplementation improved scavenging activity, reduced oxidative damage, and induced a shift towards a more anti-inflammatory milieu, in the peripheral blood of relapsing-remitting MS patients treated with Interferon-Beta1a 44 μ g, along with clinical improvements. Peripheral biomarkers of oxidative stress and inflammation could be used in small proof-of-concept studies to quickly screen the mechanisms of action of new or already-existing medications for MS.

2. State of the art

2.1 Multiple Sclerosis

2.1.1. General definition

Multiple Sclerosis (MS) is a chronic inflammatory demyelinating disease of the central nervous system (CNS) affecting approximately 2.5 million people worldwide, particularly young adults and women (C. A. Dendrou *et al.*, 2015; Thompson *et al.*, 2018). Typically, diagnosis occurs around the age of 30, with symptoms including motor difficulties, visual defects, cognitive issues, and bladder/bowel dysfunction (National Multiple Sclerosis Society, 2016). Patients may become wheelchair-bound some years after diagnosis and, ultimately, fatal complications such as infections and aspirational pneumonia are common (Rodríguez-Antigüedad Zarranz *et al.*, 2014).

2.1.2 Aetiology

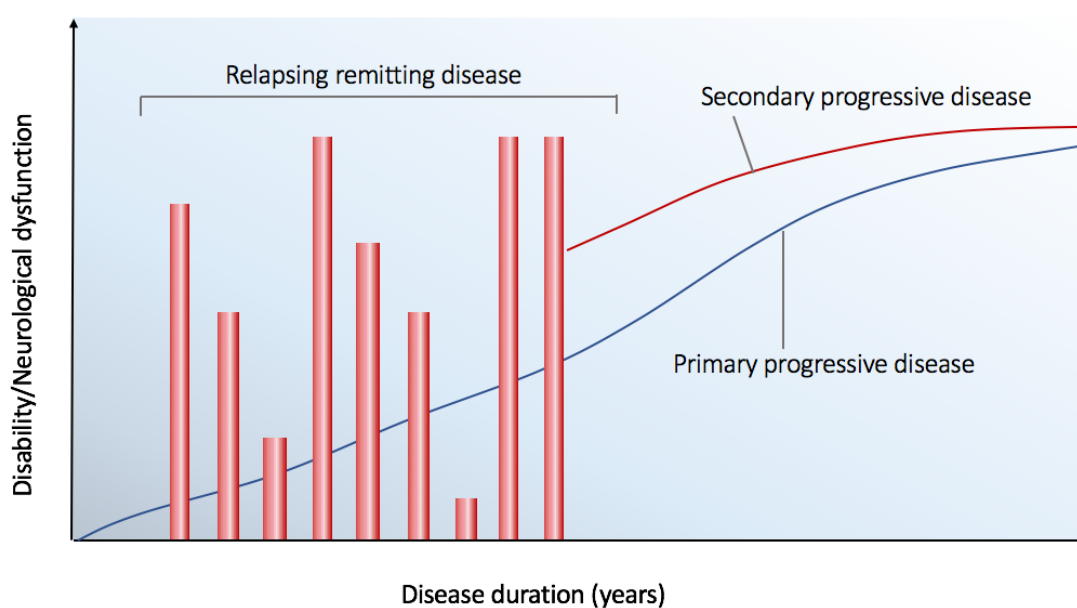
The causes of MS are unknown. Genetics represent only part of the disease risk, with genes being related primarily to proteins involved in the immune system regulation (Steri *et al.*, 2017). Equally, environmental factors such as smoking and viruses (such as Epstein-Barr virus), are thought contribute to disease risk and progression (C. A. Dendrou *et al.*, 2015; Magliozzi *et al.*, 2013; M. Moccia, Lanzillo, Palladino, *et al.*, 2015).

2.1.3 Clinical phenotypes of MS

MS can be divided into 3 main clinical types: relapsing remitting MS (RRMS), primary progressive MS (PPMS), and secondary progressive MS (SPMS). Patients may initially be diagnosed with RRMS, experiencing waxing and waning of symptoms. Partial or even full recovery can occur in remission stages. After 10-15 years of RRMS, 50% patients experience secondary progressive MS (SPMS), in

which symptoms no longer relapse and remit, but remain continuously present and progress, and patients experience clinical deterioration, perpetuating over time (Correale *et al.*, 2017). Currently, there is no clear distinction between RRMS and SPMS, with transition occurring gradually over time (Lublin *et al.*, 2014). This is contrasting with primary progressive MS (PPMS) in which patients experience progressive disease from onset, with or without inflammatory features (Lublin *et al.*, 2014) (**Figure 1**).

Figure 1. Classification of MS, and disability over time. RRMS exhibits waxing and waning of neurological symptoms and disability. This may last years or even decades, before some progression to SPMS, with a constant degeneration of neurological function and increasing disability. PPMS refers to a similar degeneration, but from the onset, in the absence of a relapsing-remitting stage. *Adapted from Dendrou et al. (2015).*

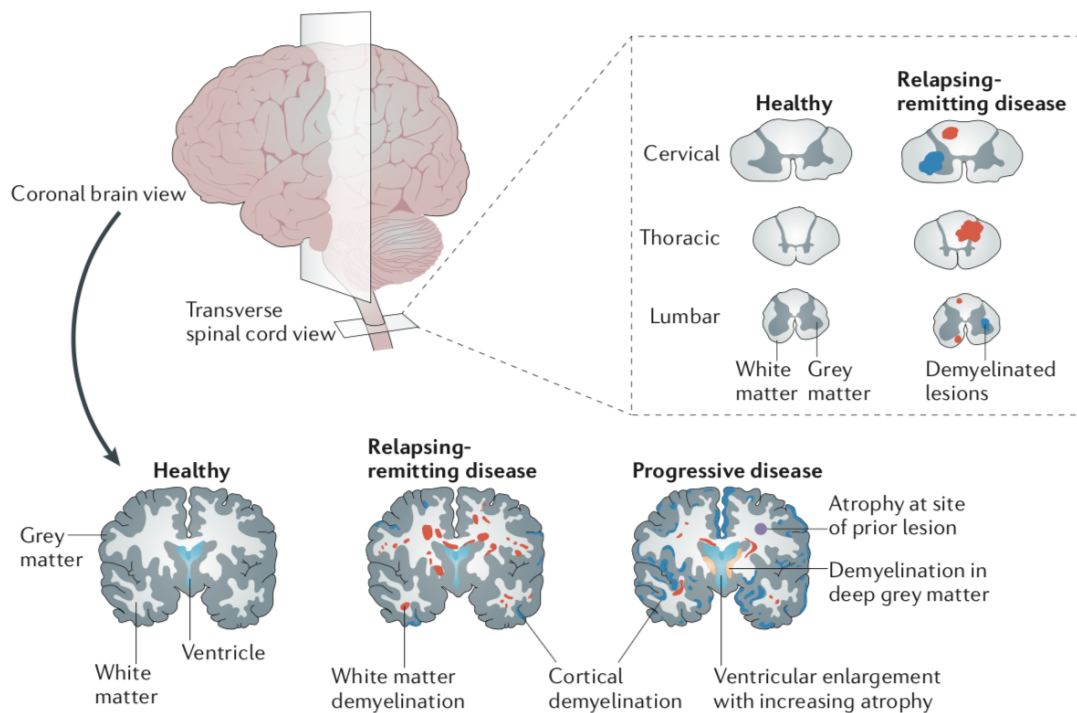


2.2 MS pathogenesis

The pathogenesis of MS remains largely unknown. It is generally accepted that MS is an immune-mediated disease with inflammatory leukocytes infiltrating the central nervous system (CNS) and ultimately leading to demyelination and neuro-axonal loss (Göbel *et al.*, 2018).

Although initial events triggering MS are currently unknown, multiple layers of pathology are observed (autoimmunity, inflammation, tissue remodelling and, more recently recognised, mitochondrial dysfunction), overall resulting in demyelination and neuronal loss, with white matter (WM) and grey matter (GM) lesions and atrophy (**Figure 2**) (C. A. Dendrou *et al.*, 2015; Magliozzi, Reynolds, *et al.*, 2018; Martinez Sosa and Smith, 2017; Nicol *et al.*, 2015). As such, a number of cells and mechanisms are involved in MS pathology within both normal-appearing (NA) and lesional WM and GM (M Moccia and Ciccarelli, 2017).

Figure 2. White and grey matter lesions in MS. RRMS exhibits a high level of WM lesions, with GM lesions occurring more in progressive disease. Previously, GM lesions were largely undetected; development of MRI technology has now revealed their prevalence to a similar degree to WM lesions, with a prominent role in disability. *Adapted from Dendrou et al., 2015*



2.2.1 Macrophages and microglia

Macrophages are innate, phagocytic antigen-presenting cells (APCs), which can activate (and are activated by) lymphocytes, through the release of cytokines influencing lymphocyte activity and generating a pro-inflammatory loop in the brain parenchyma (C. Dendrou *et al.*, 2015).

Progression of experimental autoimmune encephalomyelitis (EAE) (the most commonly used animal model of MS) is correlated to macrophage infiltration from the periphery to the CNS (Ajami *et al.*, 2011). Some studies in EAE have implicated macrophages in the initial stages of demyelination and lesion formation, with microglia following in later stages (C. Dendrou *et al.*, 2015). Indeed, microglia represent a late maturation stage of macrophages. Microglia act as the resident innate immune cells of the brain, with cytokine release, astrocyte and lymphocyte activation, and cellular debris scavenging (Prins *et al.*, 2015).

2.2.3 Astrocytes

Formerly, astrocytes were only considered relevant to MS in the formation of glial scars after lesion resolution, whilst they are currently appreciated to have a more dynamic role. Astrocytes activated by inflammation are abundant in MS, advocating their involvement from early inflammatory stages (Ponath *et al.*, 2018). In the long-term, astrocytes have been shown to heighten inflammation by releasing pro-inflammatory mediators, adhesion molecules, and chemokines, associated with microglia/macrophages migration into the parenchyma (Ponath *et al.*, 2018). A continuous crosstalk between astrocytes and microglia/lymphocytes has been documented (Legroux and Arbour, 2015).

2.2.4 T- and B-lymphocytes

Different lymphocyte subsets interact among each other and contribute to the maintaining of a pro-inflammatory milieu through the production of a variety of soluble mediators (e.g., cytokines and chemokines) (Göbel *et al.*, 2018) (**Figure 3**).

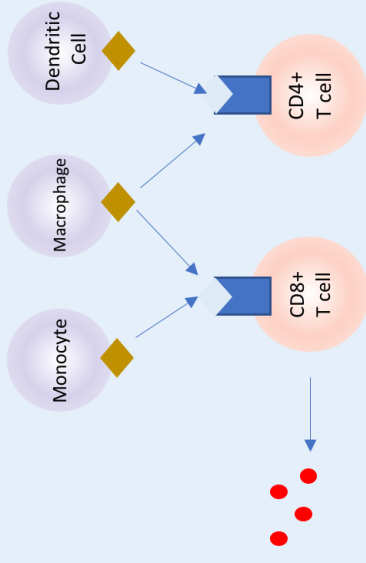
Pro-inflammatory T-lymphocytes are traditionally thought to be the key effectors in MS pathogenesis and, in keep with this, most approved MS therapies primarily target T cells by modulating their access and/or function within the CNS (Kinzel and Weber, 2016). T-lymphocytes

infiltrate the CNS in later stages of lesion formation (C. A. Dendrou *et al.*, 2015), through direct activation of resident APCs (Bartholomäus *et al.*, 2009). After invasion, these activated immune cells produce soluble mediators (e.g., cytokines and chemokines) that maintain a pro-inflammatory milieu compartmentalized within the CNS (Göbel *et al.*, 2018). From a pathological perspective, CD4⁺ (helper) T cells are more concentrated in the peri-vascular cuff, whereas CD8⁺ (cytotoxic) T cells are widely distributed within the parenchyma (Reich *et al.*, 2018).

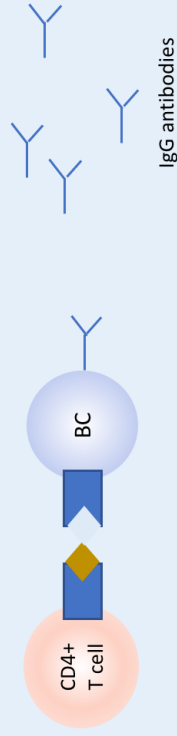
More recently, the dramatic success of B-cell-depleting antibodies in reducing MS clinical and radiological progression has shed light on the role of B-lymphocytes in MS pathogenesis (Gasperini *et al.*, 2013; Greenfield and Hauser, 2018; Kinzel and Weber, 2016). After migrating to the CNS, B cell-derived plasma cells are responsible for the production of cerebrospinal fluid (CSF)-specific antibodies (oligoclonal bands) that have diagnostic and clinical relevance (Arrambide *et al.*, 2018; Kinzel and Weber, 2016; Reich *et al.*, 2018). Also, B-lymphocytes produce a set of cytokines, chemokines and survival factors, such as tumor necrosis factor alpha (TNF- α), interferon-gamma (IFN- γ), granulocyte macrophage-colony stimulating factor (GM-CSF) and interleukin (IL)-15, that contribute to developing and maintaining a B cell-friendly milieu (Cervantes-Gracia and Husi, 2018; Kinzel and Weber, 2016; Steri *et al.*, 2017). B cells also secrete IL-6 that induces CD4⁺ T-17 differentiation and inhibits the generation of regulatory T cells (Duddy *et al.*, 2007). In the meanwhile, the ability of B cells to produce anti-inflammatory cytokines (such as IL-10) is inhibited (Kinzel and Weber, 2016). This could be important in more advanced disease stages, where infiltration of immune cells from the periphery is decreased (Howell *et al.*, 2011), and B-lymphocytes accumulate in the meninges and subpial regions, in the form of follicle-like structures (Magliozzi *et al.*, 2010). B-lymphocyte-rich follicle-like structures have been associated with a gradient of neuronal loss and demyelination, and with shorter time to wheelchair, and younger age at onset and death. (Howell *et al.*, 2011; Magliozzi *et al.*, 2007).

In the periphery

1. Innate cells
Self CNS antigens are expressed by innate immune cells. These may have processed antigens in the CNS, and drained into the blood, or express a non-self antigen with similar structure to a CNS self antigen- eliciting mimicry



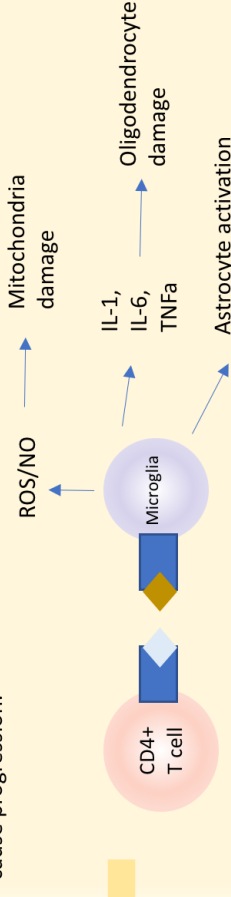
2. Activation of TCs in the periphery
TCRs recognise the antigen. Innate cells stimulate T cell maturation by cytokine release. CD8+ cells release cytokines, CD4+ cells activate BCs



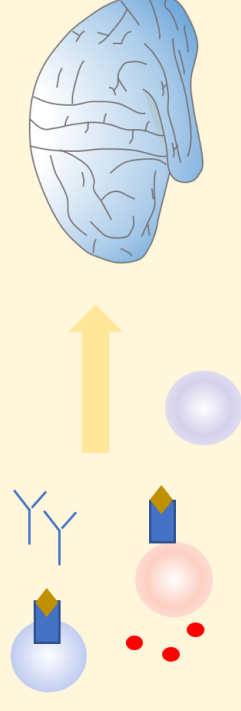
3. Activation of BCs in the periphery
TCRs recognise the antigen. Innate cells stimulate T cell maturation by cytokine release.

In the CNS

6. Feedback loop between innate cells, TC and BCs
Positive feedback loops can occur between these cells within the CNS, now regardless of the periphery, forming a micro-environment which can perpetuate disease and possibly cause progression.



5. Activation of resident microglia
These cells can activate microglia in the brain, which in turn can exacerbate T cell responses, and cause aberrant astrocyte maintenance of the BBB and excitotoxicity, oligodendrocyte and mitochondrial damage



4. Infiltration into the CNS
Antibodies, macrophages, monocytes and activated BCs and TCs can enter the brain through the CSF-meningeal pathway or breaching the BBB.

Figure 3 Immunity in the periphery and the CNS relevant to MS Whether autoimmunity is initiated in the periphery or the CNS is not known, however in either case, a feedback loop between the two may be important. Innate cells can be activated through mimicry, infiltration of antigens into the CNS or antigens escaping the CNS into the periphery. These induce inflammation and activate adaptive immunity. Due to BBB breakdown, and entry via CSF-meningeal pathway, these adaptive immune TC and BCs can enter the CNS and perpetuate inflammation and breakdown of myelin. BC: B-cell; TC: T-cell; BBB: blood-brain barrier. *Original figure.*

2.3 Magnetic resonance imaging in MS

Advances in magnetic resonance imaging (MRI) techniques have enriched our understanding of the disease. Conventional MRI has become a pivotal tool for diagnosing and clinical monitoring of MS (Thompson *et al.*, 2018). More recently, several quantitative MRI techniques have been developed, presenting with a higher specificity towards the pathological aspects of MS, when compared with conventional MRI (Filippi *et al.*, 2012; Filippi and Rocca, 2011; M Moccia and Ciccarelli, 2017).

2.3.1 Brain lesion count and volume

Lesion measures are pivotal for MS diagnosis and clinical monitoring, and include the number of gadolinium-enhancing and new/enlarging T2 lesions, and their related volumes (Tur *et al.*, 2018). Lesions are the best biomarker of active inflammation in MS, acting as a surrogate measure of clinical relapses, and allowing the screen for early disease activity in phase 2 clinical trials in RRMS (Sormani and Bruzzi, 2013). On the contrary, lesion-derived measures play a secondary -but not negligible- role in the study of progressive MS. In PPMS, the burden of T2-visible lesion load and of gadolinium-enhancing lesions is low, despite clinical severity (Miller and Leary, 2007), and seems to have only a minimal impact on the disability accrual over time (Khaleeli *et al.*, 2010).

2.3.2 Global and regional brain atrophy

Brain atrophy is detectable on MRI scans from the earliest clinical stages of MS and is a biomarker of irreversible neurodegenerative processes (Ontaneda and Fox, 2017). Global brain atrophy has been associated with the degree of disability in large cohorts of both RR and progressive MS (Khaleeli *et al.*, 2008; Rovaris *et al.*, 2008). Besides, improvements in MRI post-processing have allowed to segment WM and GM (both cortical and deep) separately, allowing refinement of association with clinical features (Fisniku *et al.*, 2008; Magliozzi, Reynolds, *et al.*, 2018; Rocca *et al.*, 2012; Scalfari *et al.*, 2018). Regional volumes might show a greater change over time (Eshaghi,

Marinescu, *et al.*, 2018; Eshaghi, Prados, *et al.*, 2018; Kapoor *et al.*, 2010), resulting in higher sensitivity and smaller sample size when compared with global measures (Healy *et al.*, 2009). Intriguingly, brain atrophy has not been associated with relapse risk in RRMS, suggesting that atrophy is probably driven more by (possibly independent) neurodegenerative changes than inflammatory lesions, which further support the use of this measure in progressive MS (Moccia, Quarantelli, *et al.*, 2017; Ontaneda and Fox, 2017).

2.3.3 Advanced MRI techniques

Conventional neuroimaging techniques lack specificity with regard to different pathophysiological substrates of MS, and are not able to explain the heterogeneous and long-term clinical evolution of the disease (Bodini *et al.*, 2015; Friese *et al.*, 2014; Popescu *et al.*, 2013; Sormani *et al.*, 2014). Advanced MRI techniques, such as magnetization transfer ratio (MTR), diffusion tensor imaging (DTI), and magnetic resonance spectroscopy (MRS), may provide higher pathological specificity for the more destructive aspects of the disease (i.e., demyelination and neuroaxonal loss), and be more closely associated with clinical correlates (Barkhof *et al.*, 2009; Enzinger *et al.*, 2015). Moreover, functional MRI (fMRI) is contributing to the definition of the role of cortical reorganization after MS tissue damage (Rocca *et al.*, 2012).

Among a variety of quantitative MRI measures, the MTR calculated from magnetization transfer (MT) imaging has emerged as a measure of particular interest. MTR values reflect the efficiency of the magnetization exchange between mobile protons in tissue water and those bound to the macromolecules, such as myelin. MTR might have a potential role in correlating with clinical and cognitive disability (Z. Khaleeli *et al.*, 2007; Ranjeva *et al.*, 2005), predicting clinical progression (Z. Khaleeli *et al.*, 2007; Khaleeli *et al.*, 2008), and monitoring treatment efficacy in MS (van den Elskamp *et al.*, 2010). In view of this, MTR has been included in several clinical trials in progressive

MS and has been measured in GM, WM, T2 lesions, putamen, thalamus and optic nerve (ClinicalTrials.gov, 2016; Connick *et al.*, 2012; Fox *et al.*, 2016; Romme Christensen *et al.*, 2014).

MRI alone provides only indirect information about the underlying pathological changes of the disease (Filippi *et al.*, 2012). Therefore, to shed light on the exact pathological substrates reflected by MRI abnormalities, correlative pathological and further MRI studies are certainly needed (Moccia, de Stefano, *et al.*, 2017).

3. Objectives

The present study aims to explore the pathogenesis of MS on *post mortem* brain samples and *in vivo*, and, in particular, has three main objectives:

1. Defining the pathology of MS with latent-profile models

In the first part of the study, we analysed *post mortem* MS brain samples with a data driven approach in order to define pathology profiles of MS, with their possible clinical correlates.

2. Pathological correlates of MTR in MS

The second part of the study is based on *post mortem* MRI and its pathological correlates. In particular, we explored pathological correlates of an advanced MRI technique (MTR), ideally designed to detect myelin content, but possibly affected by the variety of MS pathology.

3. Peripheral markers of oxidative stress and inflammation in MS

Finally, we explored the feasibility of studying (and modifying) oxidative stress and inflammation *in vivo* by measuring biomarkers in the peripheral blood.

4. Defining the pathology of multiple sclerosis with latent-profile models

4.1 Introduction

Classifications of MS ought to reflect its clinical course and, ideally, its pathological background. Accurate patient profiling is crucial for prognostic and therapeutic purposes in the clinical practice, and to recruit homogeneous populations in observational studies and clinical trials designed to address specific questions (Broman *et al.*, 1965; Ntranos and Lublin, 2016).

Current clinical classification of MS phenotypes is based on the assessment of inflammatory activity (relapses or active lesions on MRI), and of progression of disability (either together or separately) (Fred D. Lublin *et al.*, 2014). This descriptive classification fits perfectly with currently-available disease modifying treatments (DMTs) for MS that are specifically able to target inflammation (Ntranos and Lublin, 2016), and has been a cornerstone to prove their efficacy on progressive patients with inflammatory features (Hughes *et al.*, 2018; Kappos *et al.*, 2018; Montalban *et al.*, 2017).

In past decades, a number of pathological classifications have been proposed based on the degree of demyelination and immune cell interactions in lesional and peri-lesional white matter (WM) (Bö *et al.*, 1994; Bruck *et al.*, 1995; Kuhlmann *et al.*, 2017; Lassmann *et al.*, 1998; Lucchinetti *et al.*, 2000; Sanders *et al.*, 1993; Van Der Valk and De Groot, 2000). These qualitative classifications were thought to depict the temporal evolution of demyelination and inflammation (e.g., active lesions progressively becoming inactive), and shared common pathogenetic elements (Kuhlmann *et al.*, 2017; Van Der Valk and De Groot, 2000), that have been used for studying potential therapeutic targets (Lassmann, 2017). However, patterns of demyelination and inflammation across different

lesions were consistently heterogeneous between MS patients, but remained substantially homogeneous within the same patient, also in serial biopsies (Breij *et al.*, 2008; Lucchinetti *et al.*, 2000; Metz *et al.*, 2014). These findings suggest that different subgroups of MS patients share similar pathogenetic mechanisms leading to demyelinating inflammatory lesions (Breij *et al.*, 2008; Lucchinetti *et al.*, 2000).

A variety of pathogenetic mechanisms occurs in MS along with inflammation and demyelination (e.g., axonal loss, astrocyte reaction, mitochondrial damage), and involves both lesional and NA tissue in the WM and GM (Haider *et al.*, 2016; Kawachi and Lassmann, 2017; Lassmann, 2018). Thus, assuming intraindividual immunopathological homogeneity, we hypothesize that MS patients can be classified in relation to the variety of pathological changes occurring in lesional and NA WM and GM, with subsequent clinical correlates. The present study aims to: 1) define pathology profiles of MS with a data-driven approach (latent-profile analysis); 2) evaluate pathological features of each pathology profile; 3) evaluate clinical correlates of each pathology profile.

4.2 Methods

4.2.1 Subjects

Tissue for this study was provided by the United Kingdom MS Tissue Bank at the Imperial College London, under ethical approval from the National Research Ethics Committee. The study followed Human Tissue Act guidelines. All MS patients (n=16) had provided informed consent to donate tissue for MS research. Informed consent of the next of kin of the healthy subject was obtained before the inclusion of the tissue in this study. Demographic and clinical characteristics are reported in **Table 1**.

Table 1. Patients and pathology profiles.

The table shows demographic and clinical feature of MS patients and their prevalent pathology profile.

MS case	1	2	3	4	5	6	7	8	9	10	11	12	13	14	15	16
Gender	M	F	F	F	F	F	M	M	F	F	F	M	F	M	F	M
Age, years	75	61	68	66	71	53	50	64	69	75	71	66	75	65	63	66
Cause of death	SE	AP	AP	AP	SE	AP	AP	PE	AP	AP	AP	SU	AP	AP	AP	AP
Age at onset, years	60	47	22	34	35	26	35	37	29	31	51	40	38	32	47	43
System of onset	Pyr	Pyr	Sen	ON	Sen	SC	SC	SC	Sen	Sen	Cer	SC	Pyr	Sen	Cer	SC
Clinical phenotype	PP	PP	SP	SP	SP	PP	PP	SP	SP	SP	SP	SP	SP	SP	PP	SP
Time to EDSS 7.0, years	7	10	30	23	22	14	9	12	25	39	10	11	26	30	7	13
Time to EDSS 10, years	15	14	46	32	36	27	15	27	40	44	20	26	37	33	16	23
Pathology profile	2	1	1	1	1	2	2	2	3	1	1	2	3	1	2	2
Prevalence of the profile	41.6%	47.1%	48.1%	47.3%	47.8%	47.6%	50.0%	47.1%	38.5%	46.7%	58.3%	52.9%	41.2%	47.6%	41.2%	44.3%

MS: multiple sclerosis; EDSS: expanded disability status scale; M: male; F: female; SE: sepsis; AP: aspiration pneumonia; PE: pulmonary embolism; SU: suicide;

Pyr: pyramidal; Sen: sensory; ON: optic neuritis; SC: spinal cord; Cer: cerebellar; SP: secondary progressive; PP: primary progressive

4.2.2 Tissue handling and immunohistochemistry

From each brain, a single coronal cut through mammillary bodies was done to separate brain into anterior and posterior halves. Then, 1 cm-thick coronal slices were cut through the entire brain using the 1 cm guide and, for the present study, the second slice posterior to the mammillary bodies towards the occipital pole was included. Slices were immersed in 10% buffered formaldehyde solution for a minimum of seven days, allowing full fixation.

After scanning, brain slices were sectioned into different 5 mm-thick tissue blocks (each approximately 20×30 mm in size) (85 blocks in 16 cases, on average 5.3 blocks per brain slice) (**Fig 1A**). Serial sections were cut through the block at 5 µm section thickness using the Tissue-Tek AutoSection automated microtome (Sakura Finetek).

Cassettes were paraffin-embedded and immunostained by IQPath under the supervision of Prof Sebastian Brandner (UCL Queen Square Institute of Neurology, University College London). Immunostaining was performed using the Ventana Discovery XT instrument and the DAB Map detection Kit (760-124), in compliance with manufacturer instructions. Cassettes were immunostained for neuro-axonal structures (NF200), myelin (SMI94), macrophages (CD68), microglia (IBA1), B-lymphocytes (CD20), T-lymphocytes (CD3), cytotoxic T-lymphocytes (CD8), astrocytes (GFAP), and mitochondrial activity (COX4, VDAC). Slides were counterstained with hematoxylin (HE). Positive and negative controls were included initially when optimizing the stains and, then, only positive controls were included for antigens not expected to be present abundantly in the tissue. Details of immunostains are reported in **Table 2**.

Table 2. Immunostains.

The table shows details of immunostains with antibodies, targets and processing.

Antigen	Pre-treatment	Dilution	Primary antibody	Secondary antibody 1:200	Target	Source
CD20	Mild Ribo CC*	1:200	1h	32min	Neurofilaments (neuro-axonal structures)	Dako7D1
CD3	Standard CC1**	1:100	1h	32min	Myelin basic protein	Leica PA0122
CD8	Standard CC1**	1:100	1h	32min	Tissue macrophage antigen	DakoM7103
NF200	Protease 1 4'	1:200	32min	32min	Clusters of differentiation of B cells	Sigma N5389
SMI94	Extended CC1**	1:500	32min	32min	Clusters of differentiation of T cells	Covance SMI94-R
CD68	Standard Ribo CC*	1:100	1h	32min	Clusters of differentiation of cytotoxic T cells	DakoPG-M1
IBA1	Standard CC1**	1:250	1h	32min	Ionizing calcium-binding adaptor molecule 1 (microglia)	Wako 019-19741
GFAP	Protease 1 4'	1:1000	32min	32min	Glial fibrillary acidic protein (astrocytes)	DakoZ0334
COX4	Standard CC1*	1:100	1h	32min	Mitochondrial inner membrane protein (intact mitochondria)	Abcam ab14744
VDAC	Standard CC1*	1:100	1h	32min	Mitochondrial outer membrane protein (damaged mitochondria)	Abcam ab15895

*1Ribo CC: citrate-based buffer and ProClin 300.

**CC1: cell conditioning 1.

Immunostained slides were digitalized as 8-bit RGB images at 40× magnification using a Leica SCN400F slide scanner (Leica Microsystems), and analysed with Definiens Tissue Studio software 3.6 (Definiens AG, Munich, Germany) (Patodia *et al.*, 2018), with a resolution of 5× for tissue identification and a resolution of 10× for stain analysis, taking care to exclude any artefacts (e.g., breaks in the section). Images were segmented into pixels of 250×250 μm^2 (0.0625 mm^2). The intensity threshold for positive labelling was set separately for each immunostain, using an automatic histogram method accounting for variation in background stain levels (Otsu, 1979). Separate thresholds were set for HE counterstaining which allowed identification of nuclei.

For each pixel, immunostain intensity and its coordinates were exported in comma-separated values (CSV) files, including brown intensity for immunostains and blue for HE.

4.2.3 Registration

To align histology spatially, a subject-wise space was created by group-wise registration of digitized histological images, via consecutive rounds of rigid, affine and non-linear registrations, with NiftyReg (version 1.3.9) (Modat *et al.*, 2010, 2014; Pichat *et al.*, 2018).

4.2.4 Image analysis and data extraction

ROIs were manually delineated on the co-registered histology with 3D Slicer (version 4.4.0). The detection of ROIs was primarily guided by histological images with higher contrast (e.g., NF200, SMI94, GFAP, COX4, VDAC). ROI area was variable depending on the amount of included tissue. The following ROIs were drawn (number of included ROIs is reported): NAWM (n=98), WM lesions (n=62), cortical NAGM (n=89), and cortical GM lesions (n=53) (on average 2.9 ± 1.8 ROIs per block). Overall, 302 records (from different cases/controls, tissue blocks, and ROIs) were included in the statistical models.

Mean immunostain intensity (percentage of stained area) and ROI area were extracted for each ROI using FSL (version 5.0.9). For data analysis, the intensity of mitochondrial immunostains was combined as follows: percentage of damaged mitochondria = (VDAC-COX4)/VDAC (Roman *et al.*, 2005; Shoshan-Barmatz *et al.*, 2010).

4.2.5 Clinical variables

Clinical variables were extracted by a neurologist blinded to the pathological analysis, from retrospective review of detailed patients' records. Clinical variables were: functional system involved at onset (cerebellar symptoms, optic neuritis, pyramidal dysfunction, sensory symptoms, spinal cord motor dysfunction), clinical course at death (SP or PPMS), time to wheelchair dependence (expanded disability status scale -EDSS- 7.0 equivalent, measured as the time from onset to wheelchair dependence), and time to death (EDSS 10 equivalent, measured as the time from onset to death) (Howell *et al.*, 2011). Causes of death were MS-related (Cutter *et al.*, 2015). Full data are reported in **Table 1**.

4.2.6 Statistics

A latent class analysis was employed to characterize pathology subtypes in MS considering quantified pathology (aim 1). Different goodness of fit parameters (AIC, BIC, and G^2 statistics) were considered to identify the number of classes that better characterize the MS sub-populations.

Differences in stain intensity between pathology profiles (aim 2) were explored using linear mixed regression models including group indicator (pathology profile 1, 2 or 3) as main variable of interest, and using profile 1 as statistical reference. Fixed effect variables included in the model were different stains (NF200, SMI94, CD20, CD3, CD8, CD68, GFAP, IBA1, and percentage of damaged

mitochondria, measured as (VDAC-COX4)/VDAC). These models used the cassettes as unit of the analysis, with a random subject intercept to account for the nested structure of the data (cassettes nested within patients). Results are presented as coefficients (Coeff) and 95% confidence interval (95%CI).

Each patient was then classified on the basis of his/her prevalent pathology profile (**Table 1**). Clinical differences between pathology profiles (aim 3) were estimated with chi-square test for categorical variables (e.g., functional system at onset, clinical phenotype) and with ANOVA for continuous variables (e.g., time to EDSS 7.0 and EDSS 10).

Statistical analyses were performed with Stata 15.0. Statistical significance was set at $p < 0.05$.

4.3 Results

4.3.1 Pathology profiles of MS

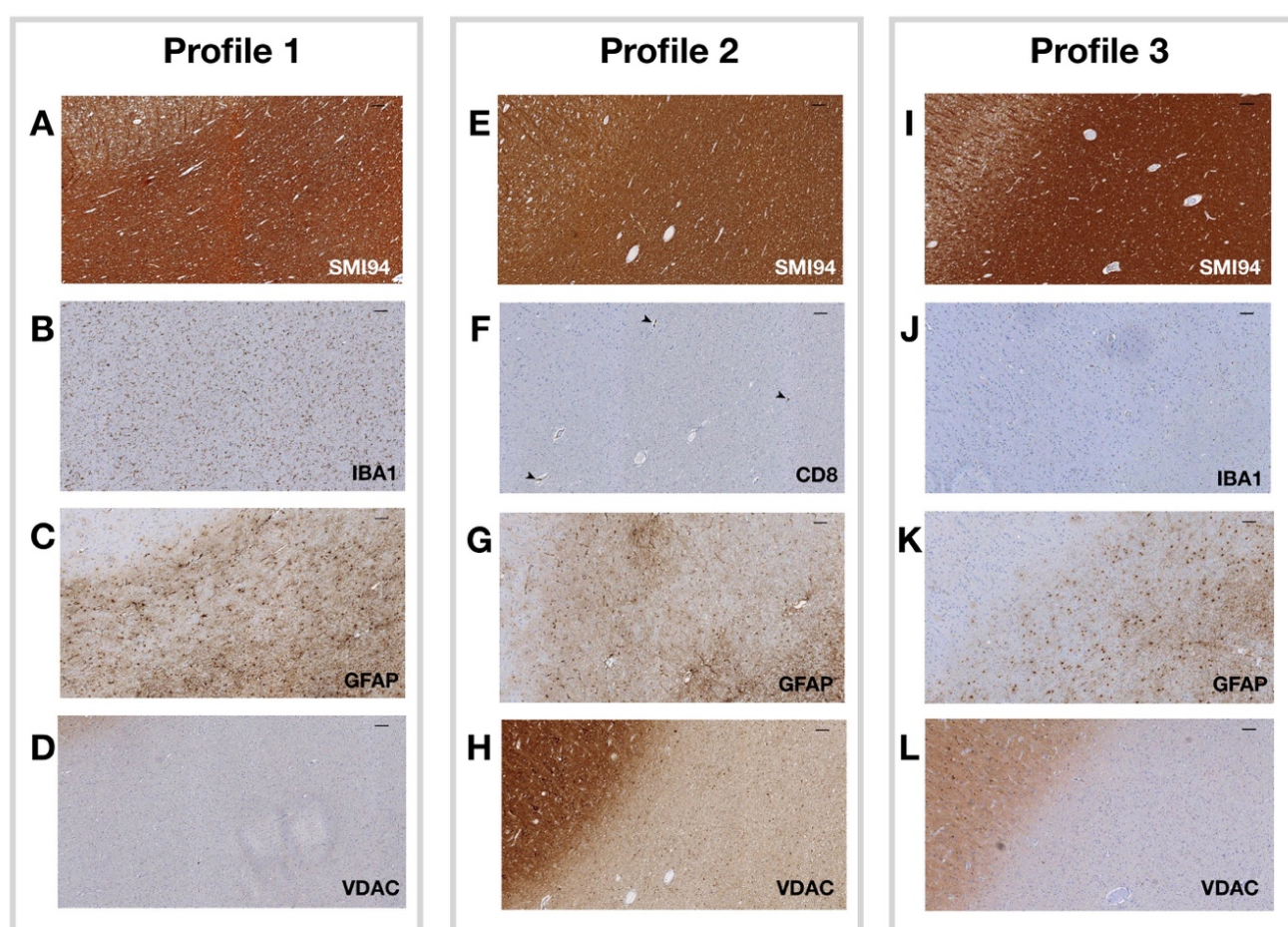
Three pathology profiles were obtained from latent profile analysis with highest goodness of fit parameters (**Figure 4**).

4.3.2 Pathological correlates of pathology profiles

When compared with **profile 1**, **profile 2** presented with lower NF200 (Coeff=-3.437; 95%CI:-6.675/-0.199; $p=0.037$), SMI94 (Coeff=-10.630; 95%CI=-13.219/-8.041; $p < 0.001$), CD68 (Coeff=-1.149; 95%CI=-1.427/-0.872; $p < 0.001$), GFAP (Coeff=-52.191; 95%CI=-56.701/-47.682; $p < 0.001$), and IBA1 (Coeff=-5.150; 95%CI=-7.074/-3.226; $p < 0.001$), and with higher CD8 (Coeff=0.877; 95%CI=0.089-1.665; $p=0.029$), and mitochondrial damage (Coeff=54.689; 95%CI=49.929/59.448; $p < 0.001$) (**Table 3; Figure 4; Figure 5**).

Figure 4. Pathology profiles.

Representative images are shown from the 3 pathology profiles. NAGM is presented in the upper left corner, with the remaining of the image being NAWM (consistently in different images/profiles). In **profile 1** (patient 11), macrophages/microglia (IBA1) and astrocytes (GFAP) infiltrates were found in the context of relatively normal myelin content (SMI94) and in the absence of mitochondrial dysfunction (VDAC) (**A-D**). In **profile 2** (patient 12), an apparently-normal myelin content (SMI94) was associated with damaged mitochondrial function (VDAC) and with cytotoxic T-lymphocytes (CD8) infiltrates (mainly perivascular, arrowheads), in absence of significant astrocyte levels (GFAP) (**E-H**). In **profile 3** (patient 9), overall levels of myelin (SMI94) were reduced, consistently with mitochondrial function (VDAC), in absence of significant infiltrates of macrophages/microglia and astrocytes (**I-L**). Scale bar is 100 μ m.



When compared with **profile 1**, **profile 3** presented with lower NF200 (Coeff=-16.798; 95%CI:-22.206/-11.391; p<0.001), SMI94 (Coeff=-41.498; 95%CI=-45.498/-37.497; p<0.001), GFAP (Coeff=-18.427; 95%CI=-25.457/-11.396; p<0.001), and IBA1 (Coeff=-5.679; 95%CI=-8.905/-2.454; p=0.001), and with higher mitochondrial damage (Coeff=26.507; 95%CI=18.864/34.151; p<0.001) (**Table 3**; **Figure 4**; **Figure 5**).

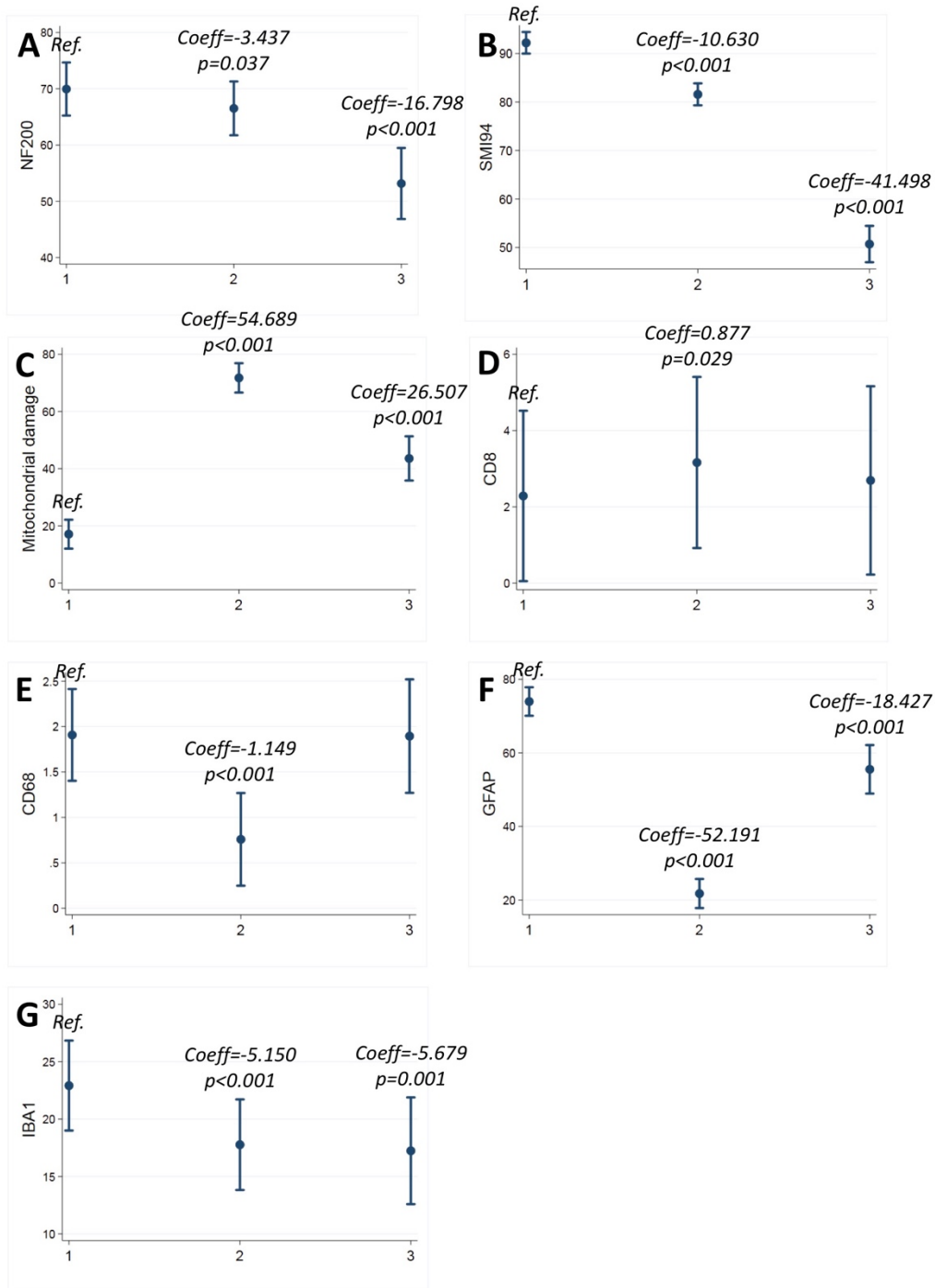
Table 3. Pathological correlates of pathology profiles.

The table shows pathological correlates of different pathology profiles. Coefficients (Coeff), 95% confidence intervals (95%CI) and p-values are shown from mixed effect regression models (with cassettes nested within patients) including group indicator (pathology profile 1, 2 or 3) as main variable of interest; profile 1 was used as reference (* indicates p<0.05).

Profile 1 <i>(reference)</i>	Profile 2				Profile 3			
	Coeff	95%CI		p-values	Coeff	95%CI		p-values
		Lower	Upper			Lower	Upper	
NF200	-3.437	-6.675	-0.199	0.037*	-16.798	-22.206	-11.391	0.026*
SMI94	-10.630	-13.219	-8.041	<0.001*	-41.498	-45.498	37.497	<0.001*
CD20	0.211	-0.284	0.706	0.403	0.077	-0.749	0.905	0.854
CD3	0.553	-0.100	1.206	0.097	0.340	-0.746	1.428	0.539
CD8	0.877	0.089	1.665	0.029*	0.408	-0.937	1.754	0.552*
CD68	-1.149	-1.427	-0.872	<0.001*	-0.012	-0.483	0.457	0.957
GFAP	-52.191	-56.701	-47.682	<0.001*	-18.427	-25.457	-11.396	<0.001*
IBA1	-5.150	-7.074	-3.226	<0.001*	-5.679	-8.905	-2.454	0.001*
Damaged mitochondria	54.689	49.929	59.448	<0.001*	26.507	18.864	34.151	<0.001*

Figure 5. Pathological correlates of pathology profiles.

Margins plots show coefficients (Coeff) and 95% confidence intervals (95%CI) from mixed effect regression models (with cassettes nested within patients) including group indicator (pathology profile 1, 2 or 3) as main variable of interest; profile 1 was used as reference; mean immunostain intensity is presented; p-values are also shown (* indicates $p < 0.05$).



4.3.3 Clinical correlates of pathology profiles

Seven patients were included in profile 1, 7 in profile 2 and 2 in profile 3, in accordance with his/her prevalent pathology profile (**Table 1**).

Most common symptoms at onset were sensory in profile 1 (57.1%), spinal cord in profile 2 (71.4%), and optic neuritis and sensory in profile 3 (50% and 50%) ($p=0.017$). Time to EDSS 7.0 was shorter in profile 2 (10.4 ± 4.5 years), when compared with profile 1 (23.4 ± 10.7 years) and 3 (25.5 ± 0.7 years) ($p=0.012$). Time to EDSS 10 was shorter in profile 2 (20.5 ± 6.8), when compared with profile 1 (32.1 ± 11.7 years) and 3 (38.5 ± 2.1) ($p=0.038$). No difference in pathology profile distribution was found between SPMS and PPMS ($p=0.237$).

4.4 Discussion

Our data driven analysis was able to detect three main profiles of MS pathology, each of which characterized by specific pathology and clinical correlates. This is the first attempt to classify MS pathology by using quantitative immunohistochemistry for a number of pathogenetic mechanisms, including NA and lesional WM and GM, applying advanced statistical methods, and validating towards clinical features of MS. The possibility to classify each MS patient into his/her pathology profile has specific clinical consequences in terms of disease profiling and treatment.

Profile 1 (active remodelling) was characterized by normal-appearing neuro-axonal structures and intact energetic metabolism, with high levels of macrophages/microglia and astrocytes, possibly contributing to subtle but continuous tissue remodelling and damage (Domingues *et al.*, 2016; Kawachi and Lassmann, 2017). Patients in profile 1 presented with relatively benign onset and mild progression, corresponding to the presence of inflammatory activity (driven by macrophages/microglia) without obvious signs of neurodegeneration (Fred D. Lublin *et al.*, 2014).

In this pathology profile, chronic tissue remodelling that macrophages/microglia and astrocytes exert, could be treated with medications modulating their function. Of note, currently available DMTs minimally affect macrophage/microglia and astrocyte function and, so, this subgroup of patients could be considered for trials with medications crossing the blood-brain-barrier and directly modulating these cells (Du *et al.*, 2017).

Profile 2 (mitochondrial dysfunction) was characterized by severely impaired mitochondrial function, along with demyelination and neuroaxonal loss, and ongoing inflammatory changes, mainly driven by cytotoxic T-cells (CD8+). Patients in profile 2 presented with severe symptoms at onset and faster disability accrual, corresponding to the presence of inflammation and neurodegeneration (Fred D. Lublin *et al.*, 2014). In this pathology profile, the ongoing inflammatory activity should be treated with immunomodulatory treatments; interventions aiming to support energetic metabolism should also be considered (Campbell and Mahad, 2018).

Finally, **profile 3 (inactive)** was characterized by severe demyelination and axonal loss, with similarly reduced mitochondrial function, without any concomitant pathological process contributing to further tissue remodelling and/or damage. Patients in profile 3 presented with relatively benign clinical features, corresponding to the absence of disease activity (Fred D. Lublin *et al.*, 2014). In this pathology profile, medications with putative neuro-regenerative effects should be evaluated.

Pathogenic mechanisms depicted by our classification are not new and have already been described and differently named in previous qualitative studies on lesional and NA MS brain tissue (**Table 4**) (Bö *et al.*, 1994; Bruck *et al.*, 1995; Kuhlmann *et al.*, 2017; Lassmann *et al.*, 1998; Lucchinetti *et al.*, 2000; Sanders *et al.*, 1993; Van Der Valk and De Groot, 2000).

Table 4. Classification of MS pathology.

The table summarise pathological features of our classification of MS pathology based on latent profile analysis, and shows its similarities to previous classifications.

Profile	Pathological features	Kuhlmann et al. <i>Acta Neuropathol</i> 2017	Haider et al. <i>Brain</i> 2016	Lucchinetti et al. <i>Ann Neurol</i> 2000	Lassmann et al. <i>J Neuroimmunol</i> 1998	Brück et al. <i>Ann Neurol</i> 1995	Bö et al. <i>J Neuroimmunol</i> 1994
1	↑↑↑ Myelin and neuro-axons	Active lesion		Pattern I and II	Inflammatory+demyelinating	Early/late	Active lesion
Active remodelling	↑ Macrophages/microglia			lesions	and inflammatory lesions	active lesion	
	↑↑↑ Astrocytes						
2	↓ Myelin and neuro-axons	Mixed	Pattern I of	Pattern III and IV	Inflammatory+demyelinating	Early/late	Chronic active
Mitochondrial	↑↑↑ Mitochondrial damage	active/inactive	neurodegeneration	lesions	and demyelinating lesions	remyelinating	lesion
dysfunction	↑ CD8+ cytotoxic T-lymphocytes	lesion				lesion	
3	↓↓↓ Myelin and neuro-axons	Inactive lesion	Pattern II of		Inactive lesion	Inactive lesion	Chronic inactive
Inactive	↑ Mitochondrial damage		neurodegeneration				lesion
	↓ Macrophages/microglia/astrocytes						

Inflammation was mainly driven by macrophages/microglia in profile 1 and CD8+ cytotoxic T-lymphocytes in profile 2. However, these cells are generally considered end-effectors of MS pathogenesis and a contribution from CD4+ T- and B-lymphocytes should be considered (C. Dendrou *et al.*, 2015; Magliozzi *et al.*, 2007; Magliozzi, Howell, *et al.*, 2018). Mitochondrial dysfunction was described in profile 2 and 3, and in both cases was associated with neuro-axonal loss. Indeed, mitochondrial damage is a marker of chronic cellular dysfunction, can exacerbate inflammation and ultimately causes neurodegeneration (Campbell and Mahad, 2018; Haider *et al.*, 2016; Lucchinetti *et al.*, 2000; Yang and Dunn, 2018). Finally, in a subset of patients (profile 3, inactive), disease activity might eventually cease, leaving signs of previous inflammatory changes (neuro-axonal loss and mitochondrial damage) without concomitant pathogenetic changes.

Limitations of the present study include reproducibility on independent and larger samples. The use of an independent sample would be helpful to reproduce our results also on tissue with different processing and by using different stains. However, latent profile models are very conservative, are data driven (and so cannot be affected by any preliminary hypothesis), and are minimally affected by sample size. Still, a larger sample size would have allowed more thoughtful clinical correlations.

In conclusion, we defined three main profiles of MS pathology characterized by subtle chronic tissue remodelling with diffuse infiltrates of macrophages/microglia and astrocytes (profile 1 – active remodelling), mitochondrial dysfunction and active inflammation (profile 2 – mitochondrial dysfunction), and chronic tissue damage in absence of active pathogenetic processes (profile 3 – inactive). Each profile presented with rather specific clinical correlates. The possibility to classify each patient depending on his/her prevalent pathology profile support the concept of MS immunopathological homogeneity within the same patient and heterogeneity between different patients. Of course, each patient presented with a dominant pathology profile (**Table 1**), but

different pathogenic mechanisms occurred at the same time. In the future, *in vivo* detection of pathology profiles should consider already existing neuroimaging techniques that are able to detect the main determinants of each profile (e.g., neuro-axonal/myelin content, microglia, and mitochondrial function) (Ciccarelli *et al.*, 2014; J. van Horsen *et al.*, 2012; Marcello Moccia and Ciccarelli, 2017).

5. Pathological correlates of magnetization transfer ratio in multiple sclerosis

5.1 Introduction

Defining the pathological specificity of MRI techniques improves their usefulness in clinical trial design and the interpretation of observational studies (Wattjes *et al.*, 2015). However, post-mortem MRI-pathological studies are scarce because of the technical challenges posed by the integration of *post mortem* MRI with histologic analysis, the difficulty in obtaining *post mortem* material, the long duration of scanning, and the need for interpretation of normal *post mortem* changes (Filippi *et al.*, 2012).

MTR is an objective index of the capacity of macromolecules to exchange magnetization with the surrounding water, indirectly estimating the extent of tissue damage (Mallik *et al.*, 2014). MTR values are lower in patients with MS than healthy controls (Bodini *et al.*, 2016), especially in patients with progressive MS, and with worse motor and cognitive disability (Stangel *et al.*, 2017). Longitudinal evaluation of MTR changes has been used to detect in-vivo a progression of MS pathology (Bodini *et al.*, 2016; Chen *et al.*, 2008), and to measure the effect of new medications in clinical trials (Brown *et al.*, 2016; Fox, 2018; Romme Christensen *et al.*, 2014).

MTR assessment in these clinical trials has been mostly interpreted as a method to probe myelin status within WM lesions (Brown *et al.*, 2016; Schwartzbach *et al.*, 2017), although axonal loss may also contribute to MTR changes in MS (Chen *et al.*, 2013; Fisher *et al.*, 2007; Moll *et al.*, 2011; Schmierer *et al.*, 2004; Schmierer, Parkes, *et al.*, 2010). Therefore, the main pathological determinant of MTR changes remain unclear.

We aimed to identify the main histologic correlate(s) of MTR and to investigate whether they varied between lesions and NA WM and GM by applying a novel methodology to align MRI to histology (Pichat *et al.*, 2018), on a large sample of patient and healthy control brain tissue, with comprehensive histology analysis.

5.2 Methods

5.2.1 Subjects

Tissue for this study was provided by the United Kingdom MS Tissue Bank at the Imperial College London, under ethical approval from the National Research Ethics Committee. The study followed Human Tissue Act guidelines. All MS patients (n=16) and controls (n=4) had provided informed consent to donate tissue for MS research. Informed consent of the next of kin of the healthy subject was obtained before the inclusion of the tissue in this study. The methods are summarized in **Figure 6**.

5.2.2 Tissue handling

From each brain, a single coronal cut through mammillary bodies was done to separate brain into anterior and posterior halves. Then, 1 cm-thick coronal slices were cut through entire brain using the 1 cm guide and, for the present study, the second slice posterior to the mammillary bodies towards the occipital pole was included. Slices were immersed in 10% buffered formaldehyde solution for a minimum of seven days, allowing full fixation.

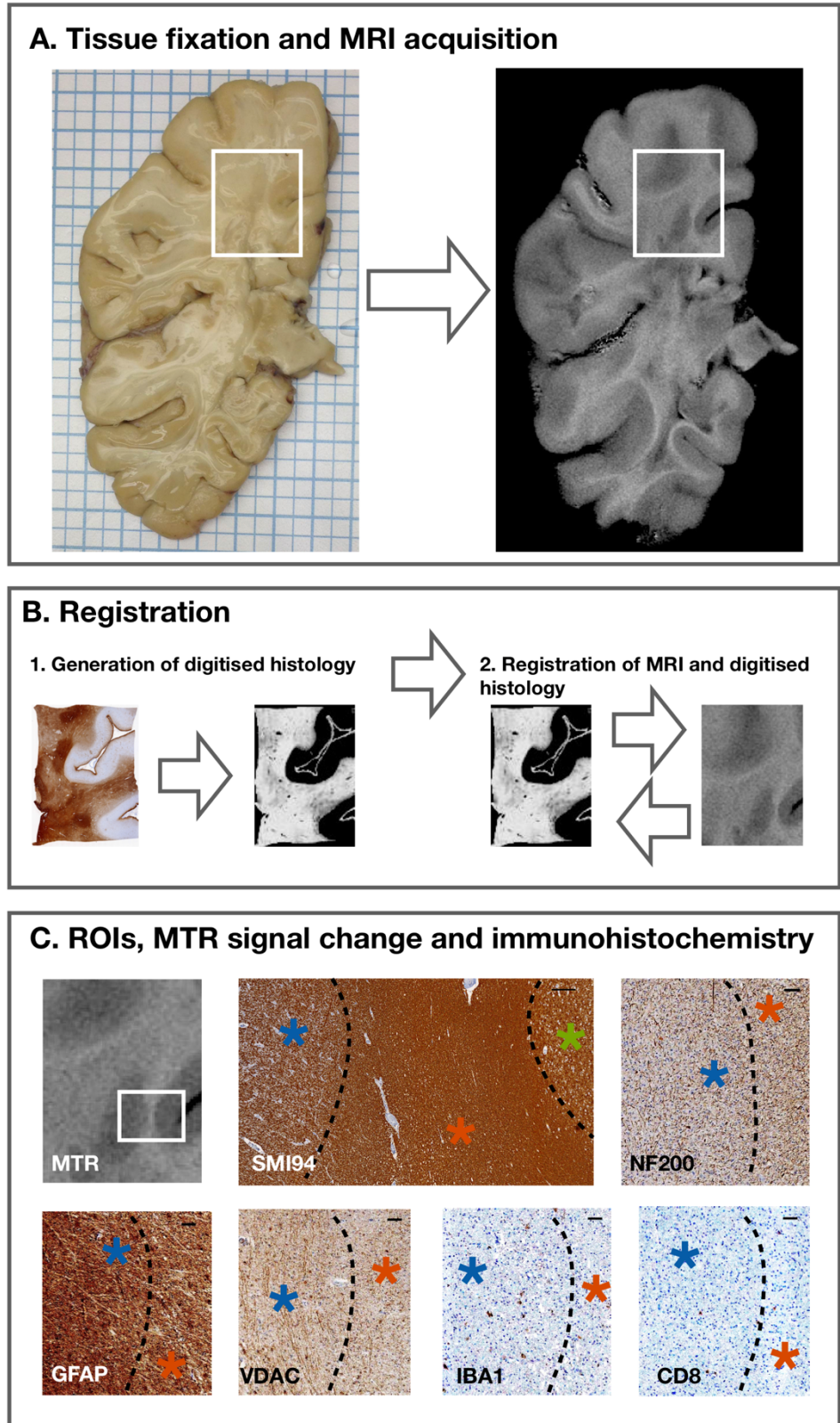
Figure 6. Tissue fixation, MRI acquisition, immunohistochemistry, registration and ROI definition.

In (A), a fixed brain slice on the left and its corresponding MTR image on the right are shown. Several tissue blocks were obtained from each slice, based on MRI and visual inspection. An example of a cassette is shown in the white box.

In (B), digitized quantifiable histological images are shown; they were generated for each stain and aligned spatially (1).

MRI images were then registered to the space of digitized quantified histological images (2). In (C), different ROIs were

analysed on both MRI and immunohistochemistry. MTR image and its corresponding immunohistochemistry (white box) are presented. Higher MTR signal corresponded to compact myelin (SMI94, scale bar 250 μ m) in NAWM (red asterisk), followed by WM lesion (blue asterisk), and NAGM (green asterisk). In WM lesions, there was reduction in neuro-axonal structures (NF200, scale bar 50 μ m), astrocyte infiltrates (GFAP, scale bar 50 μ m), and impaired mitochondrial function (VDAC, scale bar 50 μ m), compared with NAWM. Also, infiltrates of microglia/macrophages and cytotoxic T-cells were studied (IBA1 and CD8, respectively, scale bar 50 μ m).



5.2.3 MRI acquisition

Before scanning, formalin-fixed tissue was washed thoroughly with phosphate-buffered saline (PBS), and placed flat in an MRI-compatible container made of Plexiglas and filled with PBS. The MRI plane was positioned parallel to the coronal tissue slice. Proton density-weighted (PD), T2-weighted (T2) and T1-weighted (T1) spin-echo, and gradient-echo MTR sequences were acquired using a clinical scanner (3T Philips Achieva, Philips Healthcare, Best, Netherlands) with a 32-channel head coil and multi-transmit technology. The MRI acquisition included the whole 1 cm-thick tissue slice. For MTR measurement, two sets of images were obtained using a 3D slab-selective FFE sequence with two echoes (TE1/TE2=5.5/12.7ms), with (M_s) and without (M_0) sinc-Gaussian shaped MT pulses of nominal $\alpha=360^\circ$, offset frequency 1 kHz. Then, MTR maps were calculated using the standard equation: $(M_0 - M_s/M_0) \times 100$. The entire scanning protocol lasted approximately 5 hours and was run at room temperature. Further details on MRI acquisitions are given in **Table 5**.

Table 5. Parameters of MRI sequences

	Echo Time (ms)	Relaxation time (ms)	Resolution (mm)	Field of View (mm)
PD/T2	12/80	4000	0.25×0.25×2.00	160×160×16
3D-T1	6.9	15	0.50×0.50×0.50	160×160×60
MTR	5.5/12.7	37	0.25×0.25×2.00	160×160×60

MRI: magnetic resonance imaging; PD: proton density-weighted sequence; T2: T2-weighted sequence; 3D-T1: T1-weighted sequence; MTR: magnetization transfer ratio.

5.2.4 Immunohistochemistry

After scanning, brain slices were sectioned into different 5 mm-thick tissue blocks (each approximately 20×30 mm in size) (101 blocks in 20 cases/controls, on average 5.0 blocks per brain slice) (**Figure 6A**). Blocks' selection was guided by MRI and visual inspection to improve the

sensitivity of the selection process (Bö *et al.*, 2004). Serial sections were cut through the block at 5 μm section thickness using the Tissue-Tek AutoSection automated microtome (Sakura Finetek).

Cassettes were paraffin-embedded and immunostained by IQPath (University College London), under the supervision of Prof Sebastian Brandner. Immunostaining was performed using the Ventana Discovery XT instrument and the DAB Map detection Kit (760-124), in compliance with manufacturer instructions. The cassettes were immunostained and quantified for neuro-axonal structures (NF200), myelin (SMI94), macrophages (CD68), B-lymphocytes (CD20), T-lymphocytes (CD3), cytotoxic T-lymphocytes (CD8), microglia (IBA1), astrocytes (GFAP), and mitochondrial activity (COX4, VDAC). Slides were counterstained with hematoxylin (HE). Details of all immunostains are reported in **Table 2**. Positive and negative controls were included initially when optimizing the stains and, then, only positive controls were included when the antigen was not expected to be present abundantly in the tissue (e.g., CD immunostains).

Immunostained slides were then digitalized as 8-bit RGB images at 40 \times magnification using a Leica SCN400F slide scanner (Leica Microsystems) (**Figure 6B**). Digital image analysis was performed with Definiens Tissue Studio software 3.6 (Definiens AG, Munich, Germany) (Patodia *et al.*, 2018), with a resolution of 5 \times for tissue identification and a resolution of 10 \times for stain analysis, taking care to exclude any artefacts. Artefacts are excluded from the analysis (e.g., breaks in the section). Images were segmented into pixels of 250 \times 250 μm^2 (0.0625 mm^2). Considering that the degree of background staining from secondary antibodies can vary greatly among tissue blocks, the intensity threshold for positive labelling was set separately for each immunostain, using an automatic histogram method accounting for variation in background stain levels (Otsu, 1979). This histogram method finds the optimal threshold by minimizing the intraclass intensity variance, which simultaneously maximizes interclass variance. Separate thresholds were set for HE staining which

allowed identification of nuclei. Also, the use of nested statistical models further accounted for possible inter-subject variability.

For each pixel, immunostain intensity and its coordinates were exported in CSV files, including brown intensity for immunostains and blue for HE.

5.2.5 Registration

For each cassette, the following three steps were applied to obtain a 2D spatial alignment of MRI and histology (**Figure 6B**):

- 1) A subject-wise space was created by group-wise registration of digitized histological images, via consecutive rounds of rigid, affine and non-linear registrations with NiftyReg (version 1.3.9) (Modat *et al.*, 2010, 2014; Pichat *et al.*, 2018);
- 2) The T2-weighted image that best resembled a given histological image with good contrast was chosen. The selected MR plane was cropped to narrow down the search space and, then, rigid registration was performed (Modat *et al.*, 2014). Rigid registration was preferred over non-rigid to preserve the original shape of the tissue without deformation, thereby reducing the possibility of false correspondences between histology and MRI (Lee *et al.*, 2005; Pichat *et al.*, 2018);
- 3) MRI sequences were brought to the group-wise space by applying the inverse transformation from the second step to the selected planes (Modat *et al.*, 2010; Pichat *et al.*, 2018).

5.2.6 Image analysis and data extraction

Regions-of-interest (ROIs) were manually delineated on the co-registered MRI and histology with 3D Slicer (version 4.4.0). The detection of ROIs was primarily guided by T2-weighted images, with other MR and histological images used as references, to cover the full spectrum of MS pathology

(Kilsdonk *et al.*, 2016). Thus, the normal-appearing tissue was identified on MRI images, but confirmed on histological images with higher contrast (e.g., NF200, SMI94, IBA1, GFAP, COX4, VDAC) (**Figure 6C**). ROI area was variable depending on the amount of included tissue. The following ROIs were drawn (number of included ROIs is reported): NAWM (n=98), WM lesions (n=61), cortical NAGM (n=89), and cortical GM lesions (n=50) (on average 2.9 ± 1.8 ROIs per tissue block in MS, and 1.8 ± 0.4 in controls). Overall, 298 records (from different cases/controls, blocks, and ROIs) were included in the statistical models.

Mean MTR signal, mean immunostain intensity (percentage of stained area) and ROI area were extracted for each ROI using FSL (version 5.0.9). For data analysis, the intensity of mitochondrial immunostains was combined as follows: percentage of damaged mitochondria = $(VDAC - COX4) / VDAC$ (Roman *et al.*, 2005; Shoshan-Barmatz *et al.*, 2010).

5.2.7 Statistics

First, we explored population characteristics. Differences in age, gender, death-to-fixation interval and cassettes between cases and controls were measured with the chi-square test, Fisher's exact test or Mann-Whitney test, as appropriate. Differences in MTR across ROIs, when considering all patients and controls together, were measured with linear mixed regression models accounting for the hierarchical structure of data (cassettes nested within patients).

Secondly, the association between MTR and each stain (dependent variables) were explored using linear mixed regression models. Fixed-effect variables included in the model were MTR, demographics (age, gender), group indicator (case/control), factors possibly affecting MTR measurement (death-to-fixation interval, T1-weighted values corresponding to the same ROI) (Schmierer *et al.*, 2007), and factors possibly affecting histology quantification (ROI area, total cell

count as measured on HE counterstain). These models used the cassettes as the unit of the analysis, with a random subject intercept to account for the nested structure of the data (cassettes nested within patients). In a first model, we additionally fitted an interaction term between group and MTR to explore possible differences in the association of MTR and each stain between patients and controls. Similarly, an interaction term between ROI (using NAWM as reference) and MTR was set to explore possible variations in the association of MTR and each stain between different ROIs.

Finally, to assess the association between MTR and multiple stains simultaneously, so that the strongest correlate(s) of MTR values could be detected, we fitted a multivariate linear mixed regression model (assuming inter-correlation between stains). As multiple outcomes were dependent variables of this model, we selected the stains that were to be significantly associated with MTR in previous models. The multivariate linear mixed regression model was fitted using generalized structural equation modelling. Residuals were checked to confirm model assumptions. Results are presented as coefficients (Coeff), 95% confidence intervals (95%CI) and p-values.

Results were considered statistically significant if p-values were <0.05. Stata 15.0 was used for data processing and analysis.

5.3 Results

The study included 101 tissue blocks from 16 MS brains and four healthy controls, from which we derived 298 ROIs. Mean brain weight was 1241.8 ± 151.8 grams. Death-to-fixation interval was 27.1 ± 11.7 hours. Cases and controls were similar in age, gender, death-to-fixation interval, and the number of cassettes (**Table 6**). Both secondary progressive MS (n=11) and primary progressive MS (n=5) brains were studied.

Table 6. Characteristics of MS cases and healthy controls.

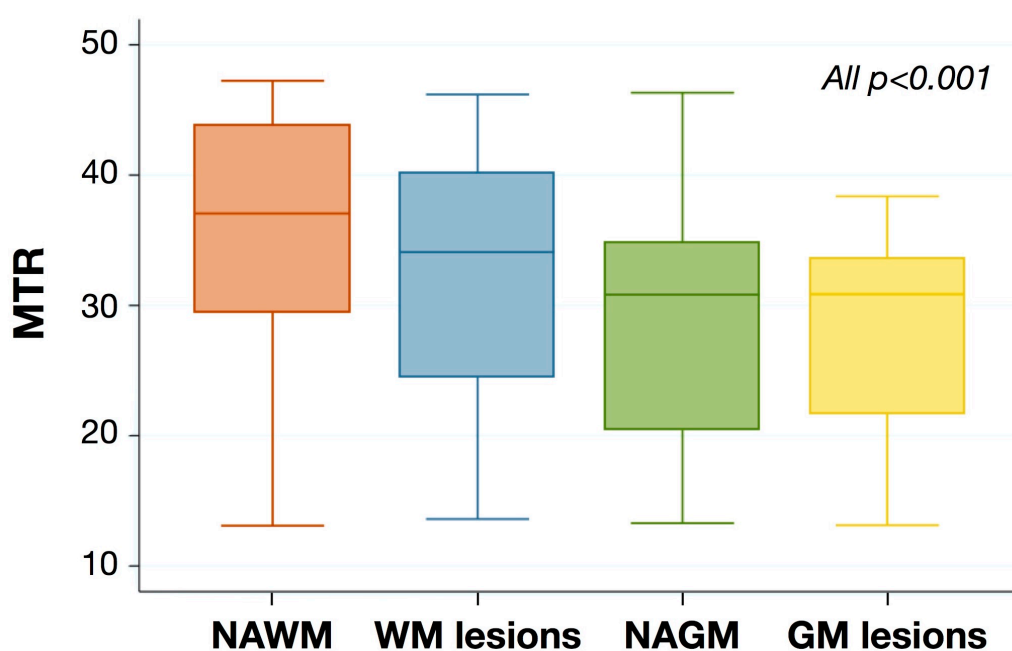
	<i>MS</i> (<i>n</i> =16)	<i>Controls</i> (<i>n</i> =4)	<i>p</i> -values
Age, years	66.1±7.1	72.5±7.8	0.199
Gender, female (%)	10 (62.5%)	2 (50.0%)	0.535
Death-to-fixation interval, hours	28.8±11.6	20.2±10.5	0.216
Cassettes, number from each slice	5.2±1.0	4.5±0.6	0.199
PPMS/SPMS, number	5/11		

P-values are shown from chi-square test, Fisher's exact test or Mann-Whitney test, as appropriate.

Considering all patients and controls together, MTR values changed across tissue classes, with higher values in NAWM (35.7±8.4), followed by WM lesions (32.5±9.0), NAGM (28.3±8.1), and GM lesions (26.2±7.4) (all $p < 0.001$) (**Figure 7**).

Figure 7. MTR values across ROIs.

Box-and-Whisker plots show mean MTR values across ROIs. P-values are shown from linear mixed regression models accounting for the hierarchical structure of data (cassettes nested within patients).



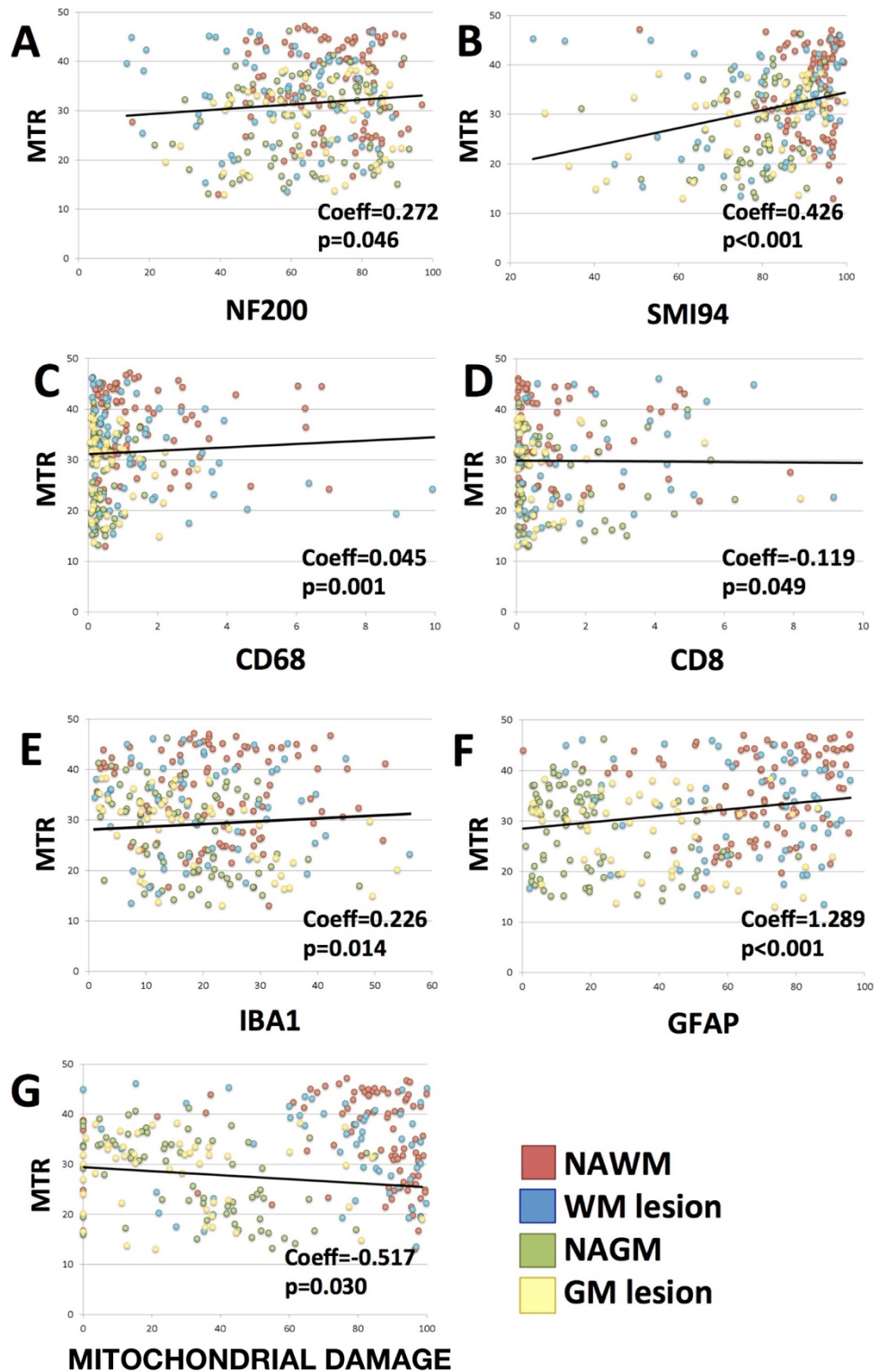
When investigating the association between MTR and histological stains in brains of patients and controls together, lower MTR values were associated with lower NF200, SMI94, CD68, IBA1, and GFAP, with higher CD8, and with a more extensive mitochondrial damage (estimated by combining VDAC and COX4). Coefficients, 95%CI and p-values are reported in **Table 7** and **Figure 8**.

When looking at the differences in the associations of MTR and histological stains between patients and controls and between ROIs, we found that the relationship between MTR and mitochondrial damage was stronger in MS brains when compared with controls (coefficients, 95%CI and p-values are reported in **Table 7**) and that the strength of the associations varied between GM and WM regions. In particular, when compared with NAWM, the association between MTR and NF200 was stronger in GM lesions, the association between MTR and SMI94 was stronger in NAGM and GM lesions, and the association between MTR and mitochondrial damage was stronger in NAGM, (coefficients, 95%CI and p-values are reported in **Table 7**). Additionally, when compared with NAWM, the association between MTR and CD68 was less strong in WM lesions, and the association between MTR and IBA1 and GFAP was less strong in NAGM and GM lesions (coefficients, 95%CI and p-values are reported in **Table 7**).

In the multivariate linear mixed regression model, MTR was independently associated with SMI94, whereas no associations were detected for the remaining stains (coefficients, 95%CI and p-values are reported in **Table 7**).

Figure 8. Associations between MTR and immunostains.

Scatter plots show associations between mean MTR values (y-axis) and mean immunostain intensity (x-axis) for NF200 (neuro-axonal structures, **A**), SMI94 (myelin, **B**), CD68 (macrophages, **C**), CD8 (cytotoxic T-lymphocytes, **D**), IBA1 (microglia, **E**), GFAP (astrocytes, **F**), and mitochondrial damage (**G**), for each ROI (NAWM in red, WM lesions in blue, NAGM in green, and GM lesions in yellow). P-values and coefficients are shown from linear mixed regression models accounting for the hierarchical structure of data (cassettes nested within patients).



5.4 Discussion

The most striking finding of our study is that myelin content was the strongest histologic correlate of MTR values, especially when MTR was measured in the GM, and this relationship was independent of all other pathological stains. Although MTR is a marker of myelin content in the GM, we found that it also has other histologic correlates, including neuro-axonal structures and mitochondrial damage in the GM, and macrophages, microglia and astrocytes in the WM. Interestingly, the association between MTR and impaired mitochondrial activity was stronger in MS cases when compared with controls, thereby expanding the list of imaging biomarkers that, at least in part, can reflect mitochondrial impairment (J. van Horsen *et al.*, 2012).

Strengths and novelties of our study, when compared with previous MRI-pathology correlation studies, are the breadth of immuno-histochemical stains, the inclusion of brains from both MS patients and healthy controls, and the analysis of both lesions and normal-appearing GM and WM. Also, our novel semi-automatic registration technique reduced the risk of false correspondence between different histology and MRI images, and ultimately enabled the study of antigens not expected to be abundantly present within brain tissue (e.g. CD8 presented with 2.7% average intensity across different ROIs).

In our dataset, MTR values correlated with markers of myelin and neuro-axonal integrity, but only myelin remained significant in a multivariate linear mixed effect model. Demyelination is a common feature of MS pathology and can occur independently from axonal loss (as shown by the presence of chronically demyelinated axons) (DeLuca *et al.*, 2006; Mottershead *et al.*, 2003; Schmierer *et al.*, 2004). Also, we found that the association between MTR and myelin content is stronger in both GM lesions and NAGM, than NAWM. Probing myelin status in the GM is of great interest considering that more axons are demyelinated in the GM (40%), when compared with WM (9%) (Carassiti *et al.*,

2017). Our findings extend previous studies where MTR was associated with myelin content and axonal loss in the GM (Chen *et al.*, 2013; Jonkman *et al.*, 2016; Schmierer, Parkes, *et al.*, 2010). Of note, MTR in WM lesions, which is frequently used as outcome measure in clinical trials (Brown *et al.*, 2016; Schwartzbach *et al.*, 2017), could reflect complex pathological changes other than myelin content (Vavasour *et al.*, 2011).

With regard to the WM, we found that lower MTR values in the WM reflected lower levels of macrophages, microglia and astrocytes. If we assume that low MTR is associated with reduced tissue integrity, this result may be seen counterintuitive considering that astrocytes make a major contribution to MS pathology by regulating macrophages and microglia towards lesional and perilesional tissue reorganization (Chang *et al.*, 2012; Correale and Farez, 2015; Howell *et al.*, 2010; Prins *et al.*, 2015). However, if MTR ranges from low values in the cerebrospinal fluid (0%) to high in compact myelin, one could argue that cellular structures, such as astrocytes, microglia and macrophages, could move MTR towards higher values, rather than lower (towards water), in particular in normal appearing and lesional WM, where these cells are more abundantly present. These cells could be responsible for abnormal MRI findings, in presence of mild demyelination or, also, in its absence (Trapp *et al.*, 2018). Of note, in the multivariate models, the association between MTR and myelin remained stable despite levels of astrocytes, microglia and macrophages, suggesting MTR is mainly driven by myelin content but can be affected by complex pathological changes occurring in the WM.

Low MTR was associated with markers of mitochondrial damage more in MS brains than controls. Mitochondrial dysfunction, with subsequent energy failure and oxidative activation, is considered as one of the main determinants of MS pathogenesis (Kawachi and Lassmann, 2017), and might contribute to the lower MTR values observed in MS patients than controls. This hypothesis might

be further tested *in vivo* by combining MTR with other imaging techniques detecting mitochondrial activity, such as quantification of N-acetyl-aspartate on MR spectroscopy (Ciccarelli *et al.*, 2014; Li *et al.*, 2013; Marcello Moccia and Ciccarelli, 2017).

The observed association between low MTR and CD8 T-lymphocyte infiltrates may reflect the presence of diffuse chronic inflammation (Frischer *et al.*, 2009). However, inflammatory cells could change in distribution depending on disease stage and ROI (Bø *et al.*, 2003; C. Dendrou *et al.*, 2015; Frischer *et al.*, 2009), and future studies will explore further the role of the levels of cytotoxic T lymphocytes in determining MTR values.

Limitations of this study include formalin fixation and *postmortem* changes in tissue structure (Schmierer *et al.*, 2008; Schmierer, Thavarajah, *et al.*, 2010). After death, T1 relaxation time shortens, and this can result in lower MTR (Schmierer *et al.*, 2007). However, we included T1-weighted values from the corresponding ROI and death-to-fixation interval as covariates in the statistical models to reduce this bias. In addition, after formalin fixation, water is removed and its contribution to the MTR signal cannot be analysed. However, in our *post mortem* sample with fixed brain tissue, MTR values were 2-3% higher than previous studies on fixed brain tissue, similar to previous studies on fresh (unfixed) brain tissue (Schmierer *et al.*, 2008; Schmierer, Thavarajah, *et al.*, 2010), and only 5-10% lower than what would be expected *in vivo* (Filippi *et al.*, 2017). Also, MTR was significantly different across ROIs, with higher values being found in NAWM, followed by WM lesions, NAGM and GM lesions (**Figure 7**), as previously described both *in vivo* and *ex vivo* (on fixed and unfixed brain tissue) (Abdel-Fahim *et al.*, 2014; Chen *et al.*, 2013; Schmierer *et al.*, 2008; Schmierer, Thavarajah, *et al.*, 2010). Overall, these findings suggest that we captured reasonably good quality data. Imaging co-registration is challenging for histological sections, inevitably suffering from structural deformations (Gilmore *et al.*, 2009). In the current study, we used a semi-automatic

registration technique to align MRI and histology spatially to reduce inaccuracy in ROI definition, as previously described (Lee *et al.*, 2005; Modat *et al.*, 2010, 2014). A qualitative evaluation of cellular structures and their interactions, which can provide information on the molecular and biological processes associated with MTR, is out of the scope of our study, which includes quantitative measurements of both MTR and pathological changes. When all the immunostains were included in the same model, myelin was the only significant correlate of MTR, independently from the other pathological processes.

In conclusion, myelin integrity is the strongest pathological correlate of MTR. However, MTR values in GM also reflect mitochondrial function and neuro-axonal loss, and in WM also monocyte, astrocyte and microglia density. These results can be helpful when interpreting MTR findings in different brain regions and add pathological specificity in clinical trials aiming to assess the specific effect of new medications which can impact on different pathological mechanisms in MS.

6. Peripheral markers of oxidative stress and inflammation in multiple sclerosis

6.1 Introduction

Chronic inflammation in MS is one of the processes responsible for increased oxidative stress (Friese *et al.*, 2014; Haider *et al.*, 2011; J van Horssen *et al.*, 2012). Products of oxidative damage are widespread in MS brains, and have been associated with development of inflammation, demyelination and neurodegeneration (Haider *et al.*, 2011; J van Horssen *et al.*, 2012). As such, the use of exogenous antioxidants looks particularly promising to treat MS with a multimodal approach, also including conventional DMTs (Friese *et al.*, 2014; J van Horssen *et al.*, 2012). Different antioxidant therapies have been studied in MS, with the strongest evidence coming from animal models for alpha-lipoic acid and epigallocatechin-3-gallate (Plemel *et al.*, 2015), and showed anti-inflammatory properties, along with neuroprotective and neuroregenerative effects (Adamczyk and Adamczyk-Sowa, 2016; Plemel *et al.*, 2015). Thus, targeting oxidative stress could represent a valuable therapeutic target for both relapsing-remitting (RR) and progressive MS (De Angelis *et al.*, 2018).

Coenzyme Q10 (CoQ10) is a cofactor of the mitochondrial oxidative respiratory chain and acts as a powerful anti-oxidant and anti-inflammatory compound and, when administered peripherally (e.g. oral or intravenous), is able to cross the blood-brain barrier (Belousova *et al.*, 2016; Spindler *et al.*, 2009). MS patients, in particular those with more severe disease, presented with lower blood levels of CoQ10 and, more in general, with higher levels of oxidative stress, when compared with controls (Choi *et al.*, 2018; Gironi *et al.*, 2014). When supplementing MS patients with CoQ10 during a 12-week period, a reduction in peripheral markers of oxidative stress (Sanoobar *et al.*, 2013), and

inflammation was noted (Sanoobar *et al.*, 2015), along with improvement of fatigue and depressive symptoms (Sanoobar, P Dehghan, *et al.*, 2016).

However, most protocols on anti-oxidant therapies in MS included a limited set of laboratory and clinical outcomes of MS (Plemel *et al.*, 2015). Thus, we utilized a wide set of laboratory and clinical measures to explore: 1) the effect of CoQ10 supplementation along with Interferon-Beta1a 44µg treatment on variations of markers of oxidative stress and inflammation in the peripheral blood (primary endpoint); 2) the effect of CoQ10 supplementation along with Interferon-Beta1a treatment on variations of clinical measures of MS severity (secondary endpoint); 3) the associations between variations of laboratory measures as for CoQ10 supplementation, and clinical outcomes (tertiary endpoint). Finally, in a *post-hoc* analysis of this study, we aimed to define most promising peripheral biomarkers of oxidative stress and inflammation by estimating the sample size needed to detect their significant variations.

6.2 Methods

6.2.1 Study design

This is a retrospective analysis on prospectively collected data, recorded at the MS Clinical Care and Research Centre of the “Federico II” University (Naples, Italy). Biological materials and clinical data were collected during clinical visits performed according to clinical practice. The study was approved by the “Federico II” University Ethics Committee and patients gave informed consent to the study.

Patients having received Interferon-Beta1a alone or with CoQ10 were extracted and assigned to either Group1 (CoQ10 supplementation along with Interferon-Beta1a over the first 3 months, followed by Interferon-Beta1a alone for 3 months) or Group 2 (Interferon-Beta1a alone over the first 3 months, followed by CoQ10 supplementation along with Interferon-Beta1a for 3 months),

with a crossover design, in order to obtain groups with similar demographic and clinical features (**Table 8**). This design used within-subjects comparison of treatments and, so, minimised confounding by removing any natural biological variation that may have occurred in the measurement of the outcome measures (Sedgwick, 2014).

The use of CoQ10 was open label, with patients being aware if on treatment, and no washout between the two periods was considered. To minimise any possible bias, our primary outcomes were laboratory-based (not affected by the open label design), and were recorded at the end of the treatment period; also, a near-immediate switch of treatments was considered (3 months) (Sedgwick, 2014). Details of the study design are reported in **Figure 9**.

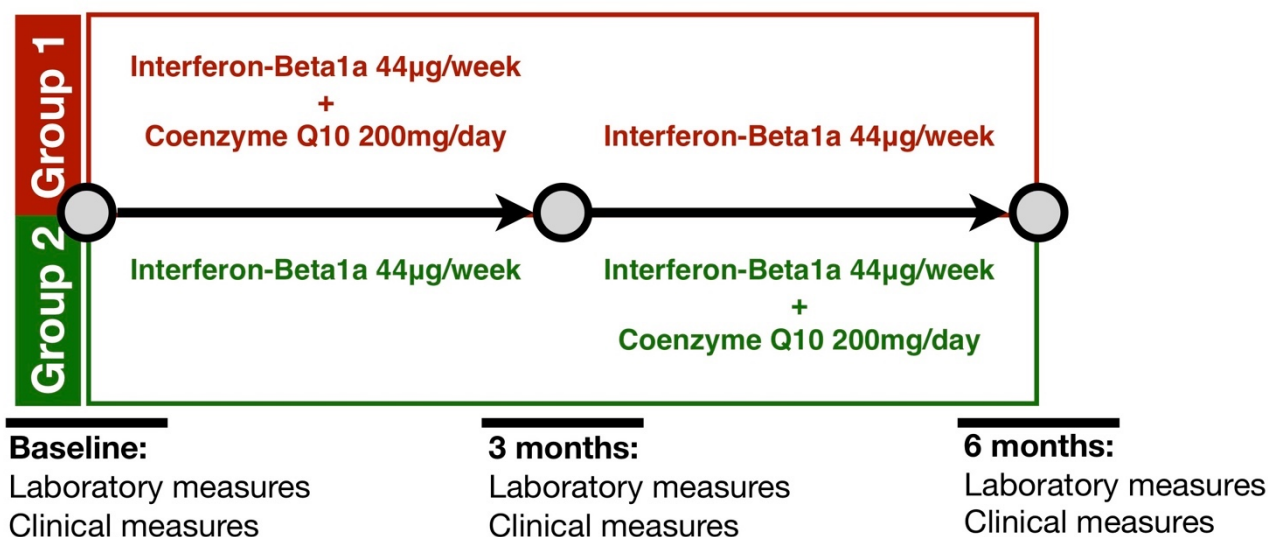
Table 8. Baseline demographic and clinical features.

Table shows demographic and clinical features of treatment groups at baseline. Group1 received CoQ10 supplementation along with Interferon-Beta1a over the first 3 months, followed by Interferon-Beta1a alone for 3 months; Group 2 received Interferon-Beta1a alone over the first 3 months, followed by CoQ10 supplementation along with Interferon-Beta1a for 3 months. P-values are reported from χ^2 test, Fisher's exact test or t-test (p<0.05 is presented as *).

	Group 1 (n=30)	Group 2 (n=30)	p-values
Age, years	42.1±10.5	40.9±9.0	0.639
Gender, female (%)	21 (70%)	21 (70%)	0.999
Disease duration, years	10.9±2.0	11.1±1.5	0.662
Baseline EDSS	2.7±1.0	2.6±1.0	0.943
Naïve patients, number (%)	15 (50%)	15 (50%)	0.999
Duration of Interferon-Beta1a, years	5.2±4.2	4.5±4.7	0.912

Figure 9. Study design.

A crossover design was considered. Group 1 received CoQ10 supplementation along with Interferon-Beta1a over the first 3 months, followed by Interferon-Beta1a alone for 3 months; Group 2 received Interferon-Beta1a alone over the first 3 months, followed by CoQ10 supplementation along with Interferon-Beta1a for 3 months.



6.2.2 Population and CoQ10 supplementation

Patients had dietary supplementation with 200mg/day CoQ10 during a 3-month period (**Figure 9**). Ubidecarenone formulation was used in compliance with indications for clinical practice (Skatto®, 100mg/ml, Chiesi Farmaceutici SpA).

Inclusion criteria were: 1) clinical and radiological diagnosis of RRMS with 2010 Revisions to the McDonald criteria (Fred D. Lublin *et al.*, 2014; Polman *et al.*, 2011); 2) age >18-year-old; 3) treatment with Interferon-Beta1a 44µg. In particular, patients were required to be steadily on treatment with Interferon-Beta1a 44µg for at least 6 months before inclusion in the study and, then, for the whole study period (3+3 months); patients were either drug-naïve or previously-treated with medications other than Interferon-Beta1a 44µg (1:1).

Exclusion criteria were: 1) recent relapse or corticosteroid treatment (<6 months); 2) exposure at any time to azathioprine, cladribine, cyclophosphamide, cyclosporine A, methotrexate, or any other immunosuppressive agent; 3) history of malignancy, major systemic disease or other illness that would in our opinion interfere with the interpretation of study results; 4) use of contraceptive drugs; 5) use of any vitamins, minerals or other over-the-counter compounds; 6) concomitant inclusion in any other observational or interventional study.

6.2.3 Laboratory outcomes

Blood samples have been collected in fasting conditions in lithium heparin tubes. Blood was immediately centrifuged and plasma samples were stored at -80°C for a maximum period of 6 months. Four cc plasma have been processed in order to analyse:

- Markers of free radical scavenging activity: uric acid (UA) and bilirubin were measured by using the UA2 and the BILTS enzymatic methods, respectively, with the COBAS® c501 analyser (Roche Diagnostic, Mannheim, Germany);
- Markers of serum oxidative damage: 8-hydroxy-2-deoxyguanosine (8-OHdG, an end product of oxidative DNA damage) and protein carbonyls (an end product of oxidative protein damage) were measured by using the OxiSelect™ Oxidative DNA Damage ELISA kit, and the OxiSelect™ Protein Carbonyl ELISA Kit, respectively (Cell Biolabs, San Diego, CA, USA);
- Markers of inflammation: the Human Cytokine Magnetic 35-Plex Panel (Invitrogen by Thermo Fisher Scientific) was used for the quantitative detection of EGF, Eotaxin, basic-FGF, G-CSF, GM-CSF, HGF, IFN- α , IFN- γ , IL-1 α , IL-1 β , IL-1RA, IL-2, IL-2R, IL-3, IL-4, IL-5, IL-6, IL-7, IL-8, IL-9, IL-10, IL-12, IL-13, IL-15, IL-17A, IL-17F, IL-22, IP-10, MCP-1, MIG, MIP-1 α , MIP-1 β , RANTES, TNF- α , and VEGF, in compliance with manufacturer's instructions; samples were analysed with a Luminex® 200™.

CellROX[®] Orange Reagent (Life Technologies) was used for measuring intracellular reactive oxygen species (ROS) production. Peripheral blood mononuclear cells (PBMCs) were isolated by stratifying heparinized whole blood on Ficoll-Hypaque (GE Healthcare). Freshly isolated PBMCs were incubated with 5µM CellROX[®] Orange Reagent for 30 minutes in the dark at 37°C, washed three times and re-suspended in PBS. The fluorescence was quantified using FACScanto II analyser (Becton–Dickinson, San Diego, CA) and Flow-Jo software (Tree Star Inc., Ashland, OR, USA); intracellular ROS production (CellROX) was measured as percent positive cells (%) and mean fluorescence intensity (MFI).

6.2.4 Clinical outcomes

Demographic characteristics (age, gender), concomitant diseases and treatments, and MS clinical features (disease duration, occurrence of relapses, EDSS) were recorded. Examiners were certified EDSS raters. Patients were classified as drug naïve or previously-treated, in relation to the use of Interferon-Beta1a; duration of Interferon-Beta1a treatment was calculated.

6.2.5 Patient-reported outcomes.

At baseline, 3- and 6-month visits, patients were required to fill in the following questionnaires:

- MS neuropsychological questionnaire (MSNQ) is a 15-item questionnaire for self-reporting everyday life functioning, neuropsychological functioning, and mood, with higher scores indicating a more preserved cognitive function; this is a quick screening tool for cognitive impairment (Benedict *et al.*, 2003; O'Brien *et al.*, 2007); an Italian version of the questionnaire was preliminary administered to a subset of patients and then used for this study;

- Visual analogic scale (VAS) is made of a 10cm straight line with equally distant numbers from 0 to 10, where the individual must indicate severity of pain and headache; this scale is easy-to-answer and is particularly suitable for exploratory analyses (Tur, 2016);
- Fatigue severity scale (FSS) is composed by 9 questions, with higher scores indicating a more severe impact of fatigue on daily life activities; this is an easy-to-answer questionnaire that can be quickly administered in the clinical practice (Tur, 2016);
- Beck's depression inventory (BDI) II consists of 21 items assessing severity of common depressive symptoms; for each item, participants are required to choose the point scale (from 0 to 3) that best describes how they felt in the last 2 weeks, with higher scores indicating the presence of depressive symptoms (Beck *et al.*, 1996).

For each scale, we preferred to use absolute values rather than cut-off points. This is because patient-reported outcomes were a secondary endpoint of the study and, accordingly, our inclusion criteria did not select a population where such cut-off points would necessarily define homogenous groups. On the contrary, absolute values of these scales would better depict variations over time and in relation to treatment.

6.2.6 Preliminary sample size calculation

Considering the main outcome of the present study (variations of laboratory markers in RRMS patients evaluated at 3 different time points by using mixed-effect linear regression models), and the results obtained in our previous longitudinal study on uric acid in RRMS (M. Moccia, Lanzillo, Costabile, *et al.*, 2015), a sample of 60 subjects for a total of 180 records was considered suitable to obtain an acceptable estimate (effect size=30%; $\alpha=0.05$; power=0.9), accepting 20% missing data. The present sample is larger than previous studies investigating CoQ10 effects in MS (Sanoobar *et al.*, 2013, 2015; Sanoobar, P Dehghan, *et al.*, 2016).

6.2.7 Statistical analyses

Preliminary comparisons between treatment groups were performed with χ^2 test, Fisher's exact test or t-test, as appropriate.

To evaluate associations between CoQ10 supplementation and variations of each laboratory (primary endpoint) and clinical outcome (secondary endpoint), mixed-effect linear regression models were employed to account for multiple measures repeated within each individual (laboratory and clinical measures collected at baseline and after 3 and 6 months). The crossover model included random effects for patient id, and fixed-effects for time (baseline, 3 and 6 months) and for the visit after CoQ10 exposure (post-CoQ10 supplementation measures were collected at 3 months in Group 1, and at 6 months in Group 2), overall accounting for possible carry-over effects. An interaction term between treatment and time (continuous) was set and marginal effects were calculated, to estimate treatment-related variations of laboratory and clinical outcomes over time in both Group 1 and 2.

To evaluate associations between CoQ10-related variations of laboratory and clinical outcomes (tertiary endpoint), we selected laboratory and clinical measures being affected by CoQ10 supplementation ($p < 0.05$ in previous models). Mixed-effect linear regression models were employed to account for multiple measures repeated within each individual. An interaction term between treatment group and each laboratory measure was set and marginal effects were calculated, to estimate possible associations between CoQ10-related variations of laboratory measures and clinical outcomes.

Covariates included in the statistical models were age, gender, disease duration, duration of Interferon-Beta1a treatment, baseline EDSS and, for analysis of UA levels, creatinine. Results are presented as coefficient (Coeff), 95% confidence intervals (95%CI) and p-values. All the variables included in the model were tested for multicollinearity (variance inflation factor [VIF] smaller than 2.5). Laboratory analyses, clinical assessments, and patient-reported scales were run blind to each other. The statistician matched the datasets and was blind to treatment codes.

Finally, sample size needed to detect treatment effect on different markers of oxidative stress and inflammation was computed using the formula $n = \frac{2(Z_{\alpha} + Z_{1-\beta})^2 \sigma^2}{\Delta^2}$, where n is the required sample size per treatment arm in 1:1 controlled trials, Z_{α} and $Z_{1-\beta}$ are constant (set at 5% alpha-error and 90% power, respectively), σ is the standard deviation and Δ the estimated effect size (Altmann *et al.*, 2009). Effect size was estimated using adjusted-beta-coefficient of 3-month variation for each laboratory measure obtained with mixed-effect linear regression models from our previous study (including age, gender, disease duration, baseline EDSS, and duration of Interferon- β 1a treatment as covariates). We assumed that the observed variation, as estimated by adjusted-beta-coefficients, was the highest achievable treatment effect (100%) over 3 months. From there, with a conservative approach, we hypothesized different treatment effects (e.g., 30%, 50%, 70%, and 90%), that were smaller than the observed effect. Standard deviation was calculated from the variation of each laboratory measure after 3 months.

Stata 15.0 and Microsoft Excel were used for data processing and analysis. Results have been considered statistically significant if $p < 0.05$.

6.3 Results

60 RRMS patients were included in the study. Treatment groups were similar in age, gender, disease duration, baseline EDSS, and distribution of naïve/on-treatment patients (**Table 8**). When considering laboratory and clinical measures, missing data were less than 20%, as preliminary accounted by sample size calculation.

During the study period, 4 patients presented with a clinical relapse (6.6%), being equally distributed in CoQ10-treated and -untreated groups.

6.3.1 CoQ10 supplementation and variations of laboratory measures

After 3 months, CoQ10 supplementation was associated with increased scavenging activity (uric acid, Coeff=0.123; p=0.034), and with reduced intracellular ROS production (% , Coeff=-9.925; p=0.021; and MFI, Coeff=-523.308; p<0.001), and DNA damage (8-OHdG, Coeff=-0.630; p=0.049).

Also, after 3 months, CoQ10 supplementation was associated with increased IL-4 (Coeff=-3.883; p=0.012) and IL-13 (Coeff=3.732; p=0.006), and with reduced Eotaxin (Coeff=-18.669; p=0.042), GM-CSF (Coeff=-1.751; p=0.006), HGF (Coeff=-26.397; p=0.015), IFN- γ (Coeff=-1.526; p=0.027), IL-1 α (Coeff=-2.460; p=0.040), IL-2R (Coeff=-29.971; p=0.016), IL-9 (Coeff=-3.749; p=0.023), IL-17F (Coeff=-68.854; p=0.034), MIP-1 α (Coeff=-5.327 ; p=0.044), RANTES (Coeff=-2331.281 ; p=0.002), TNF- α (Coeff=-1.795; p=0.024), and VEGF (Coeff=-0.398; p=0.042) (**Table 9; Figure 10**).

Table 9. Variations of laboratory outcomes in relation to CoQ10 supplementation.

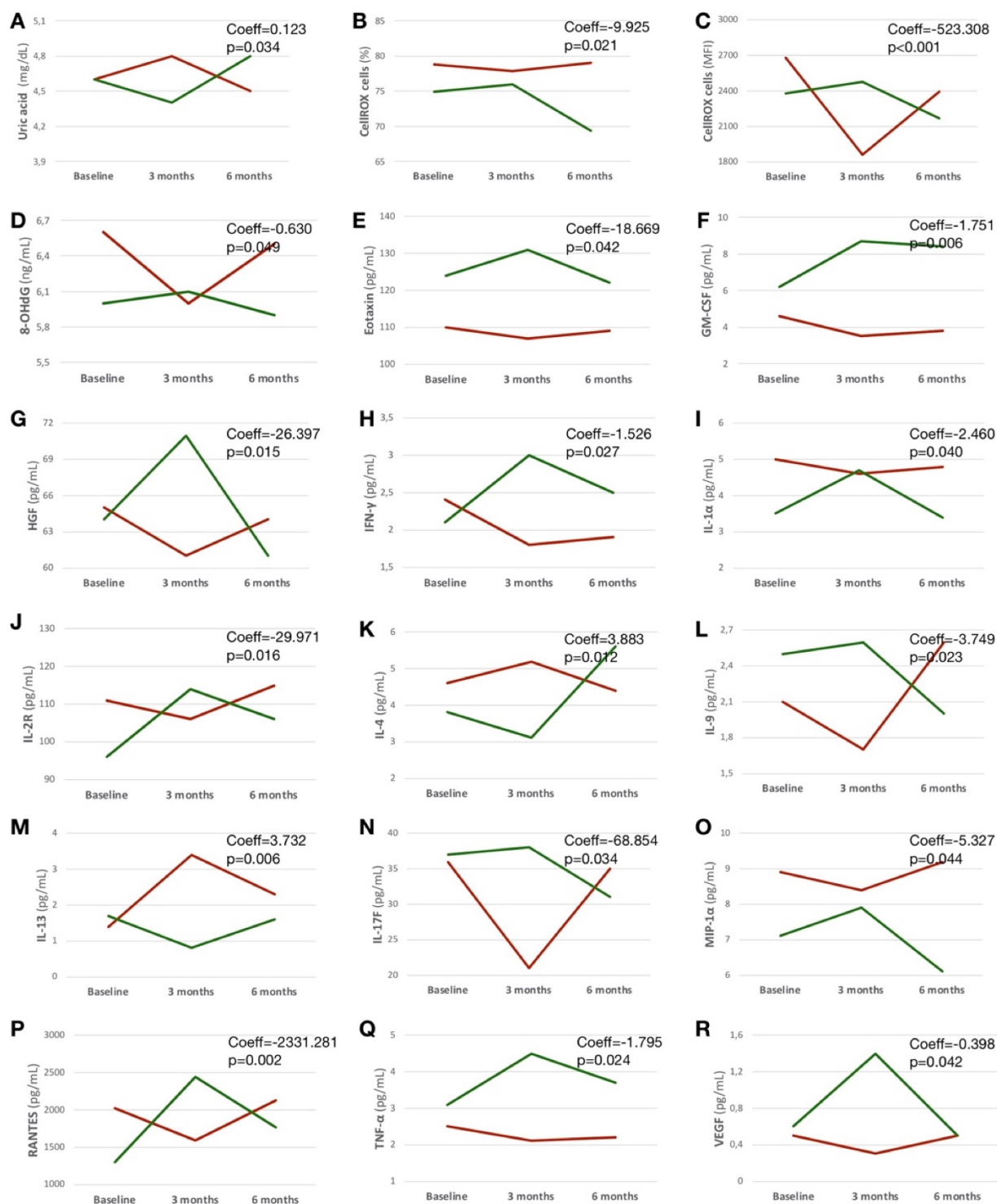
Table shows variations of different laboratory outcomes after coenzyme Q10 supplementation along with Inteferon-Beta1a, compared with Inteferon-Beta1a alone. Laboratory measures repeated within each individual at baseline and after 3 and 6 months were included in mixed-effect linear regression models where we set an interaction term between time and treatment period (post-CoQ10 supplementation visit was at 3 months in Group 1, and at 6 months in Group 2). Coefficients (Coeff), 95% confidence intervals (95%CI) and p-values are reported (p<0.05 is presented as *).

Primary endpoints	Coeff	95%CI		p-values
		<i>Lower</i>	<i>Upper</i>	
Markers of scavenging activity				
Uric acid, mg/dL	0.123	0.009	0.237	0.034*
Bilirubin, mg/dL	0.066	-0.042	0.174	0.232
Markers of oxidative damage				
CellROX cells, %	-9.925	018.353	-1.497	0.021*
CellROX cells, MFI	-523.308	-758.793	-287.822	<0.001*
Protein carbonyls, nmol/mg	-0.266	-1.320	0.787	0.620
8-OHdG, ng/mL	-0.630	-1.294	-0.034	0.049*
Markers of inflammation				
EGF, pg/mL	-3.637	-17.291	10.016	0.602
Eotaxin, pg/mL	-18.669	-36.643	-0.695	0.042*
Basic-FGF, pg/mL	-2.736	-24.007	18.535	0.801
G-CSF, pg/mL	-4.692	-16.508	7.124	0.436
GM-CSF, pg/mL	-1.751	-2.959	-0.455	0.006*
HGF, pg/mL	-26.397	-56.213	-13.418	0.015*
IFN-α, pg/mL	1.780	-22.515	26.077	0.886
IFN-γ, pg/mL	-1.526	-2.878	-0.175	0.027*
IL-1α, pg/mL	-2.460	-5.313	-0.591	0.040*
IL-1β, pg/mL	-1.188	-3.531	1.153	0.320
IL-1RA, pg/mL	-10.464	-38.999	18.070	0.472
IL-2, pg/mL	5.099	-11.619	21.817	0.550

IL-2R , pg/mL	-29.971	-54.330	-5.612	<i>0.016*</i>
IL-3 , pg/mL	28.661	-68.832	126.155	<i>0.564</i>
IL-4 , pg/mL	3.883	0.843	6.923	<i>0.012*</i>
IL-5 , pg/mL	-12.890	-34.403	8.621	<i>0.240</i>
IL-6 , pg/mL	5.559	-46.568	57.687	<i>0.834</i>
IL-7 , pg/mL	-16.428	-42.050	9.193	<i>0.209</i>
IL-8 , pg/mL	-11.418	-23.830	0.993	<i>0.071</i>
IL-9 , pg/mL	-3.749	-8.057	-1.557	<i>0.023*</i>
IL-10 , pg/mL	1615.546	-1399.093	4630.185	<i>0.294</i>
IL-12 , pg/mL	2.498	-11.569	16.566	<i>0.728</i>
IL-13 , pg/mL	3.732	1.045	6.419	<i>0.006*</i>
IL-15 , pg/mL	21.693	-37.211	80.597	<i>0.470</i>
IL-17A , pg/mL	-0.453	-1.508	0.602	<i>0.400</i>
IL-17F , pg/mL	-68.854	-140.017	-12.307	<i>0.034*</i>
IL-22 , pg/mL	-8.406	-68.069	51.255	<i>0.782</i>
IP-10 , pg/mL	5.699	-44.344	55.743	<i>0.823</i>
MCP-1 , pg/mL	39.540	-45.290	124.371	<i>0.361</i>
MIG , pg/mL	-5.409	-19.197	8.379	<i>0.442</i>
MIP-1α , pg/mL	-5.327	-10.515	-0.138	<i>0.044*</i>
MIP-1β , pg/mL	17.125	-49.443	83.695	<i>0.614</i>
RANTES , pg/mL	-2331.281	-3772.510	890.052	<i>0.002*</i>
TNF-α , pg/mL	-1.795	-3.595	-0.468	<i>0.024*</i>
VEGF , pg/mL	-0.398	-0.821	-0.052	<i>0.042*</i>

Figure 10. Laboratory outcomes.

Profile plots show variations of laboratory outcomes over time in relation to the use of Interferon-Beta1a alone or in combination with Coenzyme Q10 (Group 1: group receiving Coenzyme Q10 from baseline to 3-month follow-up is in red; Group 2: group receiving Coenzyme Q10 from 3- to 6-month follow-up is in green). Coefficients (Coeff) and p-values are shown from mixed-effect linear regression models where an interaction term between treatment and time was set and marginal effects were calculated.



6.3.2 CoQ10 supplementation and variations of clinical outcomes

After 3 months, CoQ10 supplementation was associated with reduction of EDSS (Coeff=-0.227; $p=0.036$), FSS (Coeff=-4.527; $p=0.027$), BDI (Coeff=-3.544; $p=0.022$), and VAS for pain (Coeff=-1.318; $p=0.049$) (Table 10; Figure 11).

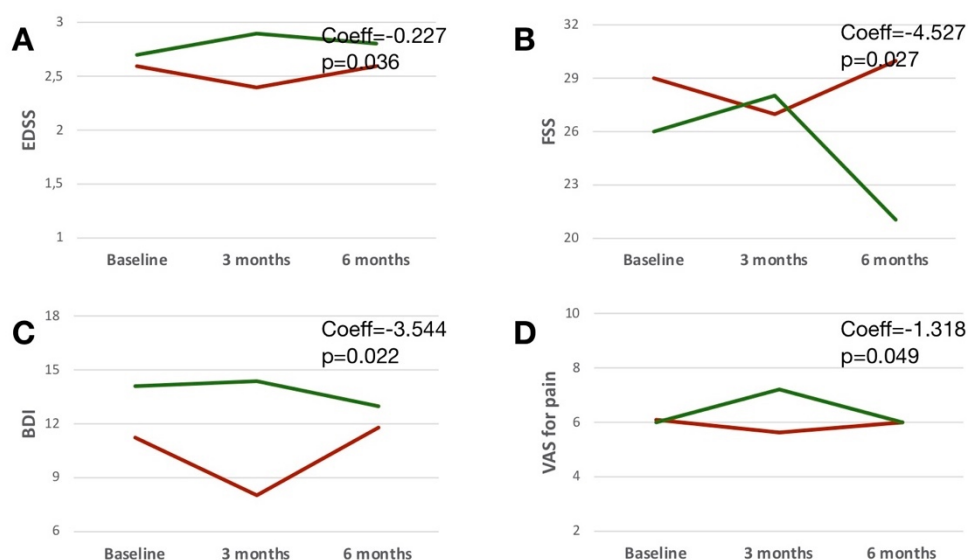
Table 10. Variations of clinical and patient-reported outcomes in relation to CoQ10 supplementation.

Table shows variations of different clinical and patient-reported outcomes (range of scales is reported) after coenzyme Q10 supplementation along with Inteferon-Beta1a, compared with Inteferon-Beta1a alone. Clinical measures repeated within each individual at baseline and after 3 and 6 months were included in mixed-effect linear regression models where we set an interaction term between time and treatment period (post-CoQ10 supplementation visit was at 3 months in Group 1, and at 6 months in Group 2). Coefficients (Coeff), 95% confidence intervals (95%CI) and p-values are reported ($p<0.05$ is presented as *).

<i>Secondary endpoints</i>	<i>Coeff</i>	<i>95%CI</i>		<i>p-values</i>
		<i>Lower</i>	<i>Upper</i>	
Clinical outcomes				
EDSS (0-10)	-0.227	-0.438	0.015	0.036*
Naïve patients	0.014	-0.251	0.222	0.915
Patient-reported outcomes				
MSNQ (0-60)	1.946	-3.655	7.548	0.496
FSS (9-63)	-4.527	-9.424	-1.368	0.027*
BDI (0-63)	-3.544	-7.212	-1.124	0.022*
VAS for pain (0-10)	-1.318	-2.691	-0.054	0.049*
VAS for headache (0-10)	-0.909	-2.359	0.541	0.219

Figure 11. Clinical outcomes.

Profile plots show variations of clinical outcomes over time in relation to the use of Interferon-Beta1a alone or in combination with Coenzyme Q10 (Group 1: group receiving Coenzyme Q10 from baseline to 3-month follow-up is in red; Group 2: group receiving Coenzyme Q10 from 3- to 6-month follow-up is in green). Coefficients (Coeff) and p-values are shown from mixed-effect linear regression models where an interaction term between treatment and time was set and marginal effects were calculated.



6.3.3 Variations of laboratory and clinical outcomes

Reduction in EDSS was associated with CoQ10 effect on reduced intracellular ROS production (MFI, Coeff=0.001; p=0.001), and IFN- γ (Coeff=0.126; p=0.009), and on increased IL-13 (Coeff=-0.057; p=0.028). Reduction in FSS was associated with CoQ10 effect on reduced intracellular ROS production (% Coeff=0.232; p=0.023). Reduction in BDI was associated with CoQ10 effect on increased uric acid (Coeff=-1.665; p=0.049). Reduction in VAS for pain was associated with CoQ10 effect on reduced IL-1 α (Coeff=0.127; p=0.043), and RANTES (Coeff=0.001; p=0.009), and on increased IL-4 (Coeff=-0.075; p=0.024).

Full results are reported in **Table 11**.

Table 11. Variations of clinical outcomes in relation to CoQ10-related effects on laboratory measures.

Table shows variations of different clinical outcomes in relation to coenzyme Q10 (CoQ10) effects on laboratory measures. Laboratory and clinical measures repeated within each individual at baseline and after 3 and 6 months were included in mixed-effect linear regression models where we set an interaction term between time and treatment period (post-CoQ10 supplementation visit was at 3 months in Group 1, and at 6 months in Group 2). Coefficients (Coeff), 95% confidence intervals (95%CI) and p-values are reported (p<0.05 is presented as *).

Tertiary endpoints	Coeff	95%CI		p-values
		<i>Lower</i>	<i>Upper</i>	
<u>EDSS</u>				
Uric acid, mg/dL	-0.045	-0.118	0.027	0.224
CellROX cells, %	0.036	-0.059	0.133	0.457
CellROX cells, MFI	0.001	0.001	0.004	0.001*
8-OHdG, ng/mL	0.095	-0.012	0.203	0.084
Eotaxin, pg/mL	0.049	-0.037	0.136	0.268
GM-CSF, pg/mL	0.055	-0.035	0.146	0.232
HGF, pg/mL	0.052	-0.034	0.138	0.236
IFN- γ , pg/mL	0.126	0.031	0.222	0.009*
IL-1 α , pg/mL	0.047	-0.038	0.133	0.274
IL-2R, pg/mL	0.057	-0.027	0.141	0.186
IL-4, pg/mL	0.050	-0.036	0.137	0.258
IL-9, pg/mL	0.049	-0.039	0.137	0.275
IL-13, pg/mL	-0.057	-0.107	-0.006	0.028*
IL-17F, pg/mL	0.044	-0.043	0.133	0.320
MIP-1 α , pg/mL	0.050	-0.0351	0.136	0.246
RANTES, pg/mL	0.053	-0.34	0.141	0.233
TNF- α , pg/mL	0.053	-0.033	0.139	0.229
VEGF, pg/mL	0.049	-0.039	0.137	0.278
<u>FSS</u>				
Uric acid, mg/dL	-0.430	-2.244	1.383	0.642

CellROX cells, %	0.232	0.071	0,473	<i>0.023*</i>
CellROX cells, MFI	0.241	-2.015	2.498	<i>0.834</i>
8-OHdG, ng/mL	0.045	-1.777	1.868	<i>0.961</i>
Eotaxin, pg/mL	0.072	-1.707	1.853	<i>0.936</i>
GM-CSF, pg/mL	0.484	-1.428	2.397	<i>0.620</i>
HGF, pg/mL	0.060	-1.743	1.864	<i>0.948</i>
IFN-γ, pg/mL	-0.004	-1.891	1.882	<i>0.996</i>
IL-1α, pg/mL	0.006	-1.810	1.822	<i>0.995</i>
IL-2R, pg/mL	-0.029	-1.870	1.810	<i>0.975</i>
IL-4, pg/mL	0.044	-1.777	1.865	<i>0.962</i>
IL-9, pg/mL	-0.013	-1.868	1.841	<i>0.989</i>
IL-13, pg/mL	0.112	-1.708	1.933	<i>0.904</i>
IL-17F, pg/mL	0.004	-1.854	1.862	<i>0.997</i>
MIP-1α, pg/mL	0.024	-1.793	1.843	<i>0.979</i>
RANTES, pg/mL	0.141	-1.721	2.003	<i>0.882</i>
TNF-α, pg/mL	0.006	-1.823	1.836	<i>0.995</i>
VEGF, pg/mL	-0.070	-1.926	1.785	<i>0.941</i>
<u>BDI</u>				
Uric acid, mg/dL	-1.665	-3.326	-0.004	<i>0.049*</i>
CellROX cells, %	-0.205	01.664	1.253	<i>0.782</i>
CellROX cells, MFI	-0.145	-1.766	1.475	<i>0.860</i>
8-OHdG, ng/mL	0.439	-0.841	1.720	<i>0.501</i>
Eotaxin, pg/mL	0.424	-0.867	1.716	<i>0.520</i>
GM-CSF, pg/mL	0.546	-0.833	1.926	<i>0.438</i>
HGF, pg/mL	0.431	-0.864	1.727	<i>0.514</i>
IFN-γ, pg/mL	0.322	-0.993	1.637	<i>0.631</i>
IL-1α, pg/mL	0.388	-0.908	1.684	<i>0.557</i>
IL-2R, pg/mL	0.310	-0.979	1.599	<i>0.637</i>
IL-4, pg/mL	0.390	-0.894	1.674	<i>0.552</i>

IL-9, pg/mL	0.232	-1.053	1.523	0.720
IL-13, pg/mL	0.291	-1.000	1.583	0.658
IL-17F, pg/mL	0.271	-1.028	1.572	0.682
MIP-1α, pg/mL	0.365	-0.922	1.652	0.578
RANTES, pg/mL	0.170	-1.142	1.483	0.799
TNF-α, pg/mL	0.362	-0.936	1.662	0.584
VEGF, pg/mL	0.166	-1.111	1.443	0.799
<u>VAS for pain</u>				
Uric acid, mg/dL	-0.230	-0.816	0.355	0.441
CellROX cells, %	0.254	-0.329	0.838	0.393
CellROX cells, MFI	0.015	-0.629	0.660	0.963
8-OHdG, ng/mL	0.124	-0.374	0.623	0.625
Eotaxin, pg/mL	0.143	-0.370	0.657	0.585
GM-CSF, pg/mL	0.262	-0.267	0.792	0.332
HGF, pg/mL	0.156	-0.362	0.674	0.555
IFN-γ, pg/mL	0.201	-0.330	0.733	0.458
IL-1α, pg/mL	0.127	0.004	0.251	0.043*
IL-2R, pg/mL	0.164	-0.357	0.687	0.537
IL-4, pg/mL	-0.075	-0.141	-0.009	0.024*
IL-9, pg/mL	0.125	-0.395	0.646	0.636
IL-13, pg/mL	0.178	-0.335	0.692	0.497
IL-17F, pg/mL	0.140	-0.377	0.658	0.594
MIP-1α, pg/mL	0.064	-0.004	0.133	0.066
RANTES, pg/mL	0.001	0.001	0.001	0.009*
TNF-α, pg/mL	0.149	-0.366	0.664	0.570
VEGF, pg/mL	0.139	-0.385	0.664	0.603

6.3.3 Sample size estimates for peripheral biomarkers of oxidative stress and inflammation in relapsing-remitting multiple sclerosis

Setting the power at 80% and alpha at 5%, low sample size requirements to detect 70% variation from a baseline pre-treatment timepoint to a 3-month follow-up were found for IL-3 (n=1), IL-5 (n=1), IL-7 (n=4), IL-2R (n=4), IL-13 (n=6), IL-6 (n=14), IL-8 (n=22), IL-4 (n=23), RANTES (n=25), TNF- α (n=26), IL-1 β (n=27), and uric acid (n=29). Other investigated markers presented with a sample size per treatment arm larger than 30 (**Figure 12; Table 12**).

Table 12. Sample size estimates for treatment arm for 3-month variations of peripheral biomarkers of oxidative stress and inflammation.

Table shows beta-coefficients (Coeff) and standard deviations (SD) used for the sample size calculation (derived from our previous study). Sample per treatment arm is reported, hypothesizing 70% treatment effect, compared with observed treatment effect, over 3 months. Power was set at 80% and alpha at 5%.

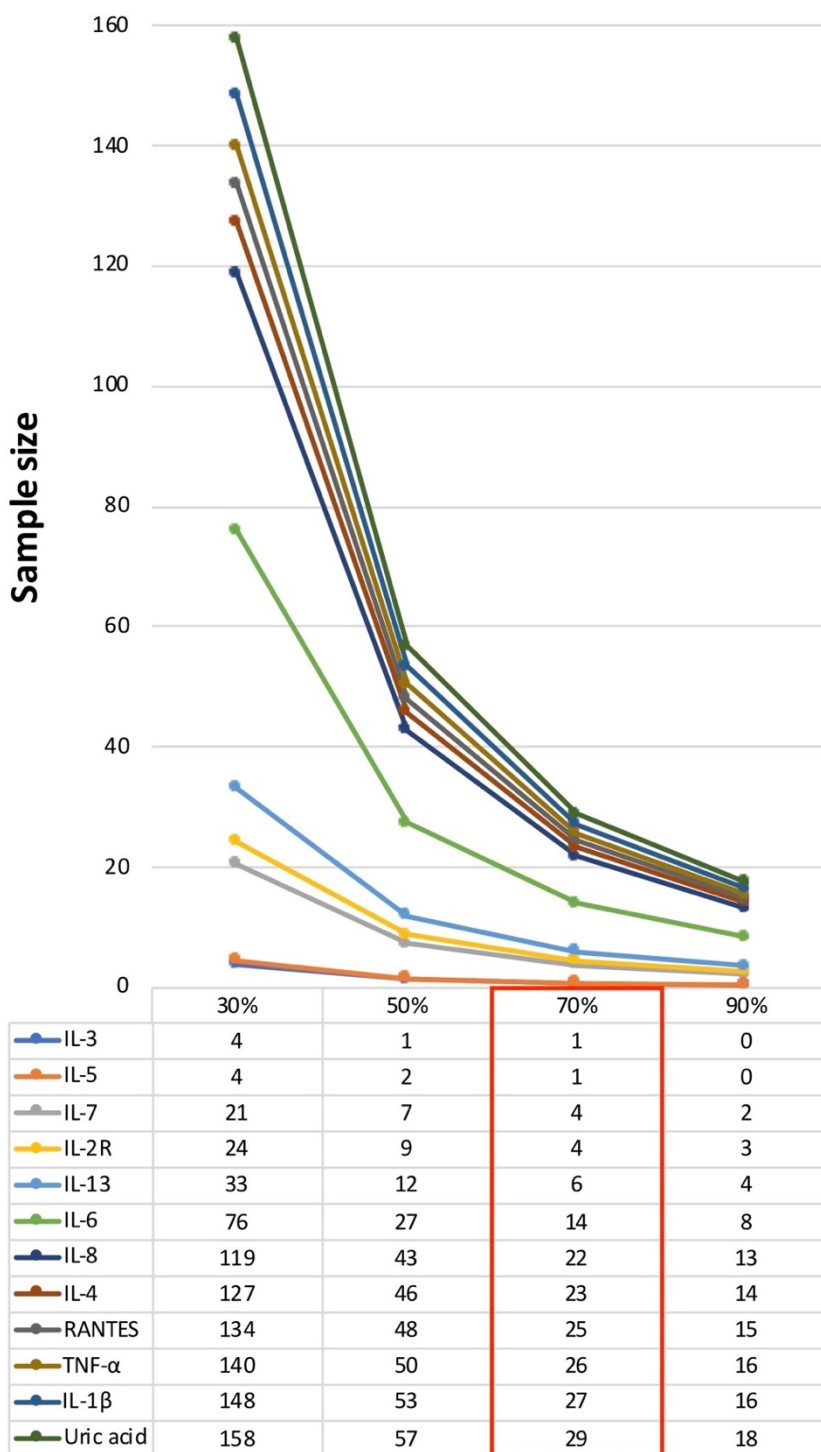
	Coeff.	SD	Sample size <i>(70% treatment effect)</i>
Markers of scavenging activity			
<i>Uric acid, mg/dL</i>	0.123	0.117	29
<i>Bilirubin, mg/dL</i>	0.066	0.190	265
Markers of oxidative damage			
<i>CellROX cells, %</i>	-9.925	11.25	41
<i>CellROX cells, MFI</i>	-523.308	1124.538	148
<i>Protein carbonyls, nmol/mg</i>	-0.266	1.393	878
<i>8-OHdG, ng/mL</i>	-0.630	0.708	40
Markers of inflammation			
<i>EGF, pg/mL</i>	-3.637	8.513	175
<i>Eotaxin, pg/mL</i>	-18.669	31.968	94

<i>Basic-FGF, pg/mL</i>	-2.736	4.863	101
<i>G-CSF, pg/mL</i>	-4.692	61.503	5498
<i>GM-CSF, pg/mL</i>	-1.751	2.524	66
<i>HGF, pg/mL</i>	-26.397	33.925	53
<i>IFN-α, pg/mL</i>	1.780	11.498	1335
<i>IFN-γ, pg/mL</i>	-1.526	1.937	52
<i>IL-1α, pg/mL</i>	-2.460	2.526	34
<i>IL-1β, pg/mL</i>	-1.188	1.096	27
<i>IL-1RA, pg/mL</i>	-10.464	18.329	98
<i>IL-2, pg/mL</i>	5.099	14.090	244
<i>IL-2R, pg/mL</i>	-29.971	11.182	4
<i>IL-3, pg/mL</i>	28.661	4.276	1
<i>IL-4, pg/mL</i>	3.883	3.317	23
<i>IL-5, pg/mL</i>	-12.890	2.069	1
<i>IL-6, pg/mL</i>	5.559	3.671	14
<i>IL-7, pg/mL</i>	-16.428	5.639	4
<i>IL-8, pg/mL</i>	-11.418	9.425	22
<i>IL-9, pg/mL</i>	-3.749	4.212	40
<i>IL-10, pg/mL</i>	1615.546	2417.951	72
<i>IL-12, pg/mL</i>	2.498	14.365	1058
<i>IL-13, pg/mL</i>	3.732	1.628	6
<i>IL-15, pg/mL</i>	21.693	21.658	32
<i>IL-17A, pg/mL</i>	-0.453	0.941	138
<i>IL-17F, pg/mL</i>	-68.854	72.039	35
<i>IL-22, pg/mL</i>	-8.406	40.134	729
<i>IP-10, pg/mL</i>	5.699	30.460	914
<i>MCP-1, pg/mL</i>	39.540	96.247	190
<i>MIG, pg/mL</i>	-5.409	13.555	201
<i>MIP-1α, pg/mL</i>	-5.327	5.338	32

<i>MIP-1β</i> , pg/mL	17.125	17.060	32
<i>RANTES</i> , pg/mL	-2331.281	2041.081	25
<i>TNF-α</i> , pg/mL	-1.795	1.608	26
<i>VEGF</i> , pg/mL	-0.398	0.519	54

Figure 12. Profile plot for sample size estimates for treatment arm.

Figure shows sample size for most promising laboratory markers of oxidative stress and inflammation (<30 patients for treatment arm, with 70% treatment effect). Sample size is reported hypothesizing 30%, 50%, 70% and 90% treatment effect. Power was set at 80% and alpha at 5%.



6.4 Discussion

Supplementation with CoQ10 in RRMS patients treated with Interferon-Beta1a 44µg was associated with improved scavenging activity, reduced oxidative damage and anti-inflammatory changes in the peripheral blood, and with clinical improvement in depressive symptoms, disability, pain and fatigue. When compared with previous investigations on the same topic, the present study included a wider set of laboratory and clinical outcomes, and attempted to relate variations in clinical measures to laboratory changes, in order to shed light on relationships between oxidative stress, inflammation and MS clinical features.

The use of CoQ10 was associated with increased levels of uric acid in the peripheral blood, a natural antioxidant responsible for a large amount of serum scavenging activity. Uric acid levels are generally lower in MS, when compared with controls, possibly as a consequence of chronic oxidative stimuli (Marcello Moccia, Lanzillo, Palladino, *et al.*, 2015). During Interferon-Beta treatment, uric acid is expected to progressively decrease, in particular in patients presenting with clinical relapses, disability progression or cognitive worsening (M Moccia, Lanzillo, Costabile, *et al.*, 2015). In our population, we might argue that antioxidant effects of CoQ10 contributed to restoring serum scavenging activity, ultimately leading to reduction of depressive symptoms, as measured by BDI. Of note, this is the first report of association between uric acid and depression in MS, whereas this has been shown already for other neurological disorders (i.e., Parkinson's disease) (Marcello Moccia, Picillo, Erro, *et al.*, 2015).

After 3-month CoQ10 supplementation, we observed an improved oxidative balance, with reduction of intracellular ROS production and of oxidative DNA damage in the peripheral blood. Oxidative damage in inflammatory cells and in DNA is a main driver of MS pathology (Haider *et al.*, 2011; J van Horsen *et al.*, 2012), and, accordingly, we found reduction of intracellular ROS production being

associated with improvement in fatigue and disability. The possibility to reduce oxidative damage and its clinical consequences by using CoQ10 along with DMTs looks particularly promising and deserves to be investigated in future studies with dedicated design.

CoQ10 supplementation reduced pro-inflammatory cytokines towards a more anti-inflammatory environment in the peripheral blood. We observed a reduction of cytokines determining chronic inflammation within the central nervous system (i.e., GM-CSF, IFN- γ , IL1- α , IL-2R, IL-9, IL-17F, TNF- α) (Becher *et al.*, 2017; C. A. Dendrou *et al.*, 2015; Elyaman and Khoury, 2017; Göbel *et al.*, 2018; Liddelw *et al.*, 2017), of chemokines suppressing the activity of microglia towards brain repair (i.e., MIP-1 α , RANTES) (Huber *et al.*, 2018; Pittaluga, 2017), and of molecules enhancing lymphocyte activity and subsequent brain damage (i.e., HGF, VEGF) (Benkhoucha *et al.*, 2013; Girolamo *et al.*, 2014; Molnarfi *et al.*, 2012). At the same time, we showed an increase of IL-4 and IL-13, that exert a neuroprotective role through suppression of pathologically-active macrophages and microglia (Göbel *et al.*, 2018; Guglielmetti *et al.*, 2016). Previous studies associated modifications towards an anti-inflammatory environment with improved clinical and radiological outcomes of MS (Magliozzi, Howell, *et al.*, 2018; Rossi *et al.*, 2017). However, we have to acknowledge that these molecules are highly related to each other (Becher *et al.*, 2017; C. A. Dendrou *et al.*, 2015; Elyaman and Khoury, 2017; Liddelw *et al.*, 2017), and direct effects of CoQ10 are hard to distinguish from its indirect, exerted through a general improvement of the oxidative balance.

Based on present results, we estimated sample size to detect significant variations for future study design. Most promising inflammatory biomarkers are strongly related to MS pathogenesis, and, in particular, to acute (e.g., IL-1 β , IL-3) and chronic inflammation (e.g., IL-2R, IL-6, IL-7, IL-8, TNF- α) within the central nervous system (Göbel *et al.*, 2018; Lee *et al.*, 2018; Lin and Edelson, 2017; Stampanoni Bassi *et al.*, 2018; Tavakolpour, 2016), to suppression of the activity of microglia

towards brain repair (i.e., RANTES), and to neuroprotective modulation of pathologically-active macrophages and microglia (e.g., IL-4, IL-13) (Göbel *et al.*, 2018; Guglielmetti *et al.*, 2016). Markers of oxidative stress also resulted in rather small sample sizes, with particular regard to markers of serum scavenging activity (uric acid), and of oxidative damage in inflammatory cells and DNA (CellROX % and 8-OHdG). Not least, biomarkers of oxidative stress and inflammation included in the present study were previously associated with MS clinical features (Göbel *et al.*, 2018; M Moccia, Lanzillo, Costabile, *et al.*, 2015; Marcello Moccia, Lanzillo, Palladino, *et al.*, 2015; Moccia *et al.*, 2018), were related to the risk of MS (Tavakolpour, 2016), and have also been used as therapeutic targets (Göbel *et al.*, 2018). Overall, peripheral biomarkers of inflammation, scavenging activity and oxidative damage gave realistically achievable sample size estimates, and could be used in exploratory clinical trials and observational studies to screen new or already existing medications with putative effects on inflammation and oxidative stress, over 3-month time. Current sample size calculations were rather conservative. We assumed observed treatment effect was 100% effect, and our estimates were based on smaller effects than what we actually observed. However, greater treatment effects could be hypothesized with different medications and doses, leading to smaller sample size.

The present study also included clinical outcomes as exploratory secondary endpoints. After CoQ10 supplementation along with Interferon-Beta1a 44µg, patients presented with lower depressive symptoms, disability, fatigue and pain. The association between CoQ10 and improvement in depression has already been described in MS (Sanoobar, Parvin Dehghan, *et al.*, 2016), and could be related to CoQ10 effects on serotonin pathways (Abuelezz *et al.*, 2017). Improvement in disability as measured by EDSS is hard to explain considering that baseline EDSS values were relatively low, study duration was 6 months and sustained changes would require longer observation time (Kalincik *et al.*, 2015). Thus, it is possible that short-term variations in EDSS could reflect physiological

fluctuations and/or were at least in part related to improvement of fatigue, as already described during CoQ10 supplementation in MS (Sanoobar, Parvin Dehghan, *et al.*, 2016), rather than a sustained improvement of disability. CoQ10 looks effective in reducing painful symptoms in other conditions (Cordero *et al.*, 2012), and its use in MS should be further explored with more appropriate scales.

The main limitation of the present study is the open-label design, considering that patients had CoQ10 supplementation according to clinical practice. However, the primary outcome of the study was the measurement of laboratory variations that cannot be influenced by the open-label design and that were associated with clinical changes. Previous studies in MS used higher CoQ10 dosage (Sanoobar *et al.*, 2013, 2015; Sanoobar, Parvin Dehghan, *et al.*, 2016); however, at 200mg/day, we were able to detect significant changes on both laboratory and clinical measures in a relatively short time. Additional markers of MS severity could have been included (e.g., MRI data), but follow-up should have been longer than 3-month treatment duration to observe meaningful changes. Some of the effects we described for CoQ10 could be attributable to Interferon-Beta1a (Molnarfi *et al.*, 2012; Zoghi *et al.*, 2011), and their separate contribution is hard to analyse; we included duration of Interferon-Beta1a in the statistical models but this did not apparently affect study results. We only collected peripheral blood but, considering that CoQ10 is able to penetrate the central nervous system (Belousova *et al.*, 2016; Spindler *et al.*, 2009), we might hypothesize that similar effects could be observed centrally.

In conclusion, the present study showed that the use of CoQ10 in RRMS patients treated with Interferon-Beta1a 44µg improved the oxidative balance and reduced the inflammatory environment in the peripheral blood, along with clinical benefits. Peripheral biomarkers of oxidative stress and inflammation could be used in exploratory, proof-of-concept studies aiming to evaluate

the profile of activity of new or already existing medications. Medications with putative anti-oxidant and anti-inflammatory effects could be tested in a short time (3 months) and on small samples (<30 per treatment arm), before being moved towards larger clinical trials requiring longer observation time and larger samples.

7. Conclusions and future perspectives

The present thesis explored MS pathogenesis comprehensively, by including both *post mortem* and *in vivo* studies, and a wide set of pathology markers. Our results can be helpful in understanding immunopathological heterogeneity of MS, in interpreting more thoughtfully MRI findings, and in designing future clinical trials and observational studies.

In the first part of the study, we applied a data-driven approach to define three profiles of MS pathology characterized by subtle chronic tissue remodelling with diffuse infiltrates of macrophages/microglia and astrocytes (profile 1 – active remodelling), mitochondrial dysfunction and active inflammation (profile 2 – mitochondrial dysfunction), and chronic tissue damage in absence of active pathogenetic processes (profile 3 – inactive). Each profile presented with rather specific clinical correlates. Afterwards, we performed pathological validation of MTR, and showed that myelin is the strongest correlate of MTR. However, MTR signal also reflects the variety of pathological changes occurring in MS and, in particular, mitochondrial function and neuro-axonal loss in GM, and monocyte, astrocyte and microglia infiltrates in WM. Finally, we showed the effect of CoQ10 on markers of oxidative stress and inflammation in the peripheral blood, suggesting that these biomarkers could be used in exploratory, proof-of-concept studies aiming to evaluate the profile of action of new or already existing medications.

In the future, knowledge acquired from our *post mortem* studies could be used for a more reliable and reproducible *in vivo* detection of MS pathology. A more thoughtful knowledge of MS pathology along with pathological validation of measures that can be acquired *in vivo*, might shed light on mechanisms of action of new medications, and could be included in clinical trials aiming to explore drug potentials for neuroprotection and tissue repair (Ruggieri *et al.*, 2017). Neuroimaging

techniques that reflect different pathology mechanisms of MS (e.g., neuro-axonal/myelin content, microglia, and mitochondrial function) (Cicarelli *et al.*, 2014; J. van Horsen *et al.*, 2012; Marcello Moccia and Ciccarelli, 2017), could be combined with biomarkers from accessible body fluids (e.g., serum or CSF) (Magliozzi, Howell, *et al.*, 2018), in order to profile the dominant pathology in each patient. Translating these results into clinical trials and practice would mean the identification of groups of patients who are more likely to respond to a medication, and the individualized monitoring of treatment response. Also, such comprehensive evaluation might help in patient stratification and, so, in further reducing the sample size needed in clinical trials by improving inclusion/exclusion criteria. This possibility is a cornerstone in patient profiling and monitoring, and in the development of life-changing treatments.

8. Acknowledgements

Present studies were the final result of a multidisciplinary work and, thus, I need to acknowledge:

- *Prof Vincenzo Brescia Morra, Dr Roberta Lanzillo, Dr Anna De Rosa, Dr Antonio Carotenuto, and Dr Roberto Albero* from the Multiple Sclerosis Clinical Care and Research Center, Department of Neuroscience, Reproductive Science and Odontostomatology, Federico II University, Naples, Italy.
- *Prof Olga Ciccarelli, Prof Alan Thompson, Prof Claudia Wheeler-Kingshott Dr Steven van de Pavert, Dr Arman Eshaghi, Dr Marios Yiannakas, and Dr Yi Wang* from the NMR Research Unit, Queen Square MS Centre, Department of Neuroinflammation, UCL Institute of Neurology, Faculty of Brain Sciences, University College London, United Kingdom.
- *Prof Frederik Barkhof* from the Department of Radiology and Nuclear Medicine, VU University Medical Center, Amsterdam, The Netherlands.
- *Prof Sebastien Ourselin, and Dr Jonas Pichat* from the Centre for Medical Image Computing, Department of Medical Physics and Bioengineering, University College London, United Kingdom.
- *Dr Raffaele Palladino* from the Department of Primary Care and Public Health, Imperial College, London, United Kingdom, and the Department of Public Health, Federico II University, Naples, Italy.

- *Prof Giuseppe Matarese, and Dr Francesco Perna* from the Laboratory of Immunology, Institute of Experimental Endocrinology and Oncology, National Research Council (IEOS-CNR), Naples, Italy, and the Treg cell Lab, Department of Molecular Medicine and Medical Biotechnologies, Federico II University, Naples, Italy.
- *Dr Fortunata Carbone* from the Neuroimmunology Unit, IRCCS Fondazione Santa Lucia, Rome, Italy.
- *Dr Teresa Micillo* from the Department of Biology, Federico II University, Naples, Italy.

Also, these studies would not have been possible without funding from ECTRIMS-MAGNIMS, UK MS Society, and Merck.

9. References

- Abdel-Fahim R, Mistry N, Mouglin O, Blazejewska A, Pitiot A, Retkute R, et al. Improved detection of focal cortical lesions using 7 T magnetisation transfer imaging in patients with multiple sclerosis. *Mult. Scler. Relat. Disord.* 2014; 3: 258–265.
- Abuelezz SA, Hendawy N, Magdy Y. Targeting Oxidative Stress, Cytokines and Serotonin Interactions Via Indoleamine 2, 3 Dioxygenase by Coenzyme Q10: Role in Suppressing Depressive Like Behavior in Rats. *J. Neuroimmune Pharmacol.* 2017; 12: 277–291.
- Adamczyk B, Adamczyk-Sowa M. New Insights into the Role of Oxidative Stress Mechanisms in the Pathophysiology and Treatment of Multiple Sclerosis. *Oxid. Med. Cell. Longev.* 2016; 2016: 1973834.
- Ajami B, Bennett JL, Krieger C, McNagny KM, Rossi FM V. Infiltrating monocytes trigger EAE progression, but do not contribute to the resident microglia pool. *Nat. Neurosci.* 2011; 14: 1142–1150.
- Altmann DR, Jaspers B, Barkhof F, Beckmann K, Filippi M, Kappos LD, et al. Sample sizes for brain atrophy outcomes in trials for secondary progressive multiple sclerosis. *Neurology* 2009; 72: 595–601.
- De Angelis F, Plantone D, Chataway J. Pharmacotherapy in Secondary Progressive Multiple Sclerosis: An Overview. *CNS Drugs* 2018; 32: 499–526.
- Arrambide G, Tintore M, Espejo C, Auger C, Castillo M, Río J, et al. The value of oligoclonal bands in the multiple sclerosis diagnostic criteria. *Brain.* 2018; 141: 1075–1084.
- Barkhof F, Calabresi PA, Miller DH, Reingold SC. Imaging outcomes for neuroprotection and repair in multiple sclerosis trials. *Nat. Rev. Neurol.* 2009; 5: 256–266.
- Bartholomäus I, Kawakami N, Odoardi F, Schläger C, Miljkovic D, Ellwart JW, et al. Effector T cell interactions with meningeal vascular structures in nascent autoimmune CNS lesions. *Nature* 2009; 462: 94–98.

Becher B, Spath S, Goverman J. Cytokine networks in neuroinflammation. *Nat. Rev. Immunol.* 2017; 17: 49–59.

Beck A, Steer R, Brown G. Beck Depression Inventory: Second Edition Manual. San Antonio (TX): The Psychological Corporation; 1996.

Belousova M, Tokareva OG, Gorodetskaya E, Kalenikova EI, Medvedev OS. Intravenous treatment with coenzyme Q10 improves neurological outcome and reduces infarct volume after transient focal brain ischemia in rats. *J. Cardiovasc. Pharmacol.* 2016; 67: 103–109.

Benedict RHB, Munschauer F, Linn R, Miller C, Murphy E, Foley F, et al. Screening for multiple sclerosis cognitive impairment using a self-administered 15-item questionnaire. *Mult. Scler.* 2003; 9: 95–101.

Benkhoucha M, Molnarfi N, Schneiter G, Walker PR, Lalive PH. The neurotrophic hepatocyte growth factor attenuates CD8+ cytotoxic T-lymphocyte activity. *J. Neuroinflammation* 2013; 10: 154.

Bö L, Geurts J, Ravid R, Barkhof F. Magnetic resonance imaging as a tool to examine the neuropathology of multiple sclerosis. *Neuropath. Appl. Neuro.* 2004; 30: 106–117.

Bö L, Mörk S, Kong PA, Nyland H, Pardo CA, Trapp BD. Detection of MHC class II-antigens on macrophages and microglia, but not on astrocytes and endothelia in active multiple sclerosis lesions. *J. Neuroimmunol.* 1994; 51: 135–146.

Bø L, Vedeler C a, Nyland H, Trapp BD, Mørk SJ. Intracortical multiple sclerosis lesions are not associated with increased lymphocyte infiltration. *Mult. Scler.* 2003; 9: 323–31.

Bodini B, Chard D, Altmann DR, Tozer D, Miller D, Thompson A, et al. White and gray matter damage in primary progressive MS: The chicken or the egg ? *Neurology* 2016; 86: 170–176.

Bodini B, Louapre C, Stankoff B. Advanced imaging tools to investigate multiple sclerosis pathology. *Press. Medicale* 2015; 44: e159–e167.

Breij ECW, Brink BP, Veerhuis R, Van Den Berg C, Vloet R, Yan R, et al. Homogeneity of active demyelinating lesions in established multiple sclerosis. *Ann Neurol.* 2008; 63: 16–25.

Broman T, Bergmann L, Fog T, Gilland O, Hyllested K, Lindberg-Broman A, et al. Aspects on classification methods in multiple sclerosis. *Acta Neurol. Scand. Suppl.* 1965; 13: 543–548.

Brown RA, Narayanan S, Stikov N, Cook S, Cadavid D, Wolansky L, et al. MTR recovery in brain lesions in the BECOME study of glatiramer acetate vs interferon β -1b. *Neurology* 2016; 87: 905–911.

Bruck W, Porada P, Poser S, Rieckmann P, Hanefeld F, Kretzschmar HA, et al. Monocyte / Macrophage Differentiation in Early Multiple Sclerosis Lesions. *Ann Neurol* 1995; 38: 788–796.

Campbell G, Mahad DJ. Mitochondrial dysfunction and axon degeneration in progressive multiple sclerosis. *FEBS Lett.* 2018; 592: 1113–1121.

Carassiti D, Altmann DR, Petrova N, Pakkenberg B, Scaravilli F, Schmierer K. Neuronal loss, demyelination and volume change in the multiple sclerosis neocortex. *Neuropathol. Appl. Neurobiol.* 2017

Cervantes-Gracia K, Husi H. Integrative analysis of Multiple Sclerosis using a systems biology approach. *Sci. Rep.* 2018; 8: 1–14.

Chang A, Staugaitis SM, Dutta R, Batt CE, Easley KE, Chomyk AM, et al. Cortical remyelination: a new target for repair therapies in multiple sclerosis. *Ann Neurol.* 2012; 72: 918–926.

Chen JT, Collins DL, Atkins HL, Freedman MS, Arnold DL, Antel JP, et al. Magnetization transfer ratio evolution with demyelination and remyelination in multiple sclerosis lesions. *Ann Neurol.* 2008; 63: 254–262.

Chen JTH, Easley K, Schneider C, Nakamura K, Kidd GJ, Chang A, et al. Clinically feasible MTR is sensitive to cortical demyelination in MS. *Neurology* 2013; 80: 246–252.

Choi I, Lee P, Adany P, Hughes A, Belliston S, Denney D, et al. In vivo evidence of oxidative stress in brains of patients with progressive multiple sclerosis. *Mult. Scler.* 2018; 24: 1029–1038.

Ciccarelli O, Barkhof F, Bodini B, Stefano N De, Golay X, Nicolay K, et al. Pathogenesis of multiple sclerosis: Insights from molecular and metabolic imaging. *Lancet Neurol.* 2014; 13: 807–822.

ClinicalTrials.gov. Dimethyl Fumarate Treatment of Primary Progressive Multiple Sclerosis

(FUMAPMS). 2016. Available from: <https://clinicaltrials.gov/ct2/show/NCT02959658>

Connick P, Kolappan M, Crawley C, Webber DJ, Patani R, Mitchell AW, et al. Autologous mesenchymal stem cells for the treatment of secondary progressive multiple sclerosis: An open-label phase 2a proof-of-concept study. *Lancet Neurol.* 2012; 11: 150–156.

Cordero MD, Cotán D, del-Pozo-Martín Y, Carrión AM, de Miguel M, Bullón P, et al. Oral coenzyme Q10 supplementation improves clinical symptoms and recovers pathologic alterations in blood mononuclear cells in a fibromyalgia patient. *Nutrition* 2012; 28: 1200–1203.

Correale J, Farez MF. The role of astrocytes in multiple sclerosis progression. *Front. Neurol.* 2015; 6: 180.

Correale J, Gaitán MI, Ysrraelit MC, Fiol MP. Progressive multiple sclerosis: from pathogenic mechanisms to treatment. *Brain.* 2017; 140: 527–546.

Cutter GR, Zimmerman J, Salter AR, Knappertz V, Suarez G, Waterbor J, et al. Causes of death among persons with multiple sclerosis. *Mult. Scler. Relat. Disord.* 2015; 4: 484–490.

DeLuca GC, Williams K, Evangelou N, Ebers GC, Esiri MM. The contribution of demyelination to axonal loss in multiple sclerosis. *Brain.* 2006; 129: 1507–1516.

Dendrou C, Fugger L, Friese M. Immunopathology of multiple sclerosis. *Nat. Rev. Immunol.* 2015; 15: 545–558.

Dendrou CA, Fugger L, Friese MA. Immunopathology of multiple sclerosis. *Nat. Rev. Immunol.* 2015; 15: 545–558.

Domingues HS, Portugal CC, Socodato R, Relvas JB. Corrigendum: Oligodendrocyte, Astrocyte and Microglia Crosstalk in Myelin Development, Damage, and Repair. *Front. Cell Dev. Biol.* 2016; 4: 71.

Du L, Zhang Y, Chen Y, Zhu J, Yang Y, Zhang HL. Role of Microglia in Neurological Disorders and Their Potentials as a Therapeutic Target. *Mol. Neurobiol.* 2017; 54: 7567–7584.

Duddy M, Niino M, Adatia F, Hebert S, Freedman M, Atkins H, et al. Distinct Effector Cytokine Profiles of Memory and Naive Human B Cell Subsets and Implication in Multiple Sclerosis. *J. Immunol.* 2007;

178: 6092–6099.

van den Elskamp IJ, Knol DL, Vrenken H, Karas G, Meijerman A, Filippi M, et al. Lesional magnetization transfer ratio: a feasible outcome for remyelinating treatment trials in multiple sclerosis. *Mult. Scler.* 2010; 16: 660–669.

Elyaman W, Khoury SJ. Th9 cells in the pathogenesis of EAE and multiple sclerosis. *Semin. Immunopathol.* 2017; 39: 79–87.

Enzinger C, Barkhof F, Ciccarelli O, Filippi M, Kappos L, Rocca MA, et al. Nonconventional MRI and microstructural cerebral changes in multiple sclerosis. *Nat. Rev. Neurol.* 2015; 11: 676–686.

Eshaghi A, Marinescu RV, Young AL, Firth NC, Prados F, Jorge Cardoso M, et al. Progression of regional grey matter atrophy in multiple sclerosis. *Brain.* 2018

Eshaghi A, Prados F, Brownlee WJ, Altmann DR, Tur C, Cardoso MJ, et al. Deep gray matter volume loss drives disability worsening in multiple sclerosis. *Ann Neurol.* 2018

Filippi M, Preziosa P, Rocca MA. Microstructural MR Imaging Techniques in Multiple Sclerosis. *Neuroimaging Clin. N. Am.* 2017; 27: 313–333.

Filippi M, Rocca MA. MR imaging of multiple sclerosis. *Radiology* 2011; 259: 659–81.

Filippi M, Rocca MA, Barkhof F, Brück W, Chen JT, Comi G, et al. Association between pathological and MRI findings in multiple sclerosis. *Lancet Neurol.* 2012; 11: 349–360.

Fisher E, Chang A, Fox RJ, Tkach JA, Svarovsky T, Nakamura K, et al. Imaging correlates of axonal swelling in chronic multiple sclerosis brains. *Ann Neurol.* 2007; 62: 219–228.

Fisniku LK, Chard DT, Jackson JS, Anderson VM, Altmann DR, Miszkiewicz K, et al. Gray matter atrophy is related to long-term disability in multiple sclerosis. *Ann Neurol.* 2008; 64: 247–254.

Fox R. A Phase II Trial of Ibudilast in Progressive Multiple Sclerosis. *AAN* 2018

Fox RJ, Coffey CS, Cudkovic ME, Gleason T, Goodman A, Klawiter EC, et al. Design, rationale, and baseline characteristics of the randomized double-blind phase II clinical trial of ibudilast in progressive multiple sclerosis. *Contemp. Clin. Trials* 2016; 50: 166–177.

Friese MA, Schattling B, Fugger L. Mechanisms of neurodegeneration and axonal dysfunction in multiple sclerosis. *Nat. Rev. Neurol.* 2014; 10: 225–38.

Frischer JM, Bramow S, Dal-Bianco A, Lucchinetti CF, Rauschka H, Schmidbauer M, et al. The relation between inflammation and neurodegeneration in multiple sclerosis brains. *Brain.* 2009; 132: 1175–1189.

Gasperini C, Haggiag S, Ruggieri S. Drugs in clinical development for multiple sclerosis: focusing on anti-CD20 antibodies. *Expert Opin. Investig. Drugs* 2013

Gilmore CP, Geurts JGG, Evangelou N, Bot JCJ, van Schijndel RA, Pouwels PJW, et al. Spinal cord grey matter lesions in multiple sclerosis detected by post-mortem high field MR imaging. *Mult. Scler.* 2009; 15: 180–188.

Girolamo F, Coppola C, Ribatti D, Trojano M. Angiogenesis in multiple sclerosis and experimental autoimmune encephalomyelitis. *Acta Neuropathol. Commun.* 2014; 2: 84.

Gironi M, Borgiani B, Mariani E, Cursano C, Mendozzi L, Cavarretta R, et al. Oxidative stress is differentially present in multiple sclerosis courses, early evident, and unrelated to treatment. *J. Immunol. Res.* 2014; 2014: 961863.

Göbel K, Ruck T, Meuth SG. Cytokine signaling in multiple sclerosis: Lost in translation. *Mult. Scler. J.* 2018; 24: 432–439.

Greenfield AL, Hauser SL. B-cell Therapy for Multiple Sclerosis: Entering an era. *Ann Neurol.* 2018; 83: 13–26.

Guglielmetti C, Le Blon D, Santermans E, Salas-Perdomo A, Daans J, De Vocht N, et al. Interleukin-13 immune gene therapy prevents CNS inflammation and demyelination via alternative activation of microglia and macrophages. *Glia* 2016; 64: 2181–2200.

Haider L, Fischer MT, Frischer JM, Bauer J, Höftberger R, Botond G, et al. Oxidative damage in multiple sclerosis lesions. *Brain.* 2011; 134: 1914–1924.

Haider L, Zrzavy T, Hametner S, Höftberger R, Bagnato F, Grabner G, et al. The topography of

- demyelination and neurodegeneration in the multiple sclerosis brain. *Brain*. 2016; 139: 807–815.
- Healy B, Valsasina P, Filippi M, Bakshi R. Sample size requirements for treatment effects using gray matter, white matter and whole brain volume in relapsing-remitting multiple sclerosis. *J Neurol Neurosurg Psychiatry*. 2009; 80: 1218–23.
- van Horssen J, Witte M, Ciccarelli O. The role of mitochondria in axonal degeneration and tissue repair in MS. *Mult. Scler*. 2012; 18: 1058–1067.
- van Horssen J, Witte M, Ciccarelli O. The role of mitochondria in axonal degeneration and tissue repair in MS. *Mult. Scler*. 2012; 18: 1058–1067.
- Howell OW, Reeves CA, Nicholas R, Carassiti D, Radotra B, Gentleman SM, et al. Meningeal inflammation is widespread and linked to cortical pathology in multiple sclerosis. *Brain*. 2011; 134: 2755–2771.
- Howell OW, Rundle JL, Garg A, Komada M, Brophy PJ, Reynolds R. Activated Microglia Mediate Axoglia Disruption That Contributes to Axonal Injury in Multiple Sclerosis. *J. Neuropathol. Exp. Neurol*. 2010; 69: 1017–1033.
- Huber AK, Giles DA, Segal BM, Irani DN. An emerging role for eotaxins in neurodegenerative disease. *Clin. Immunol*. 2018; 189: 29–33.
- Hughes J, Jokubaitis V, Lugaresi A, Hupperts R, Izquierdo G, Prat A, et al. Association of Inflammation and Disability Accrual in Patients With Progressive-Onset Multiple Sclerosis. *JAMA Neurol*. 2018
- Jonkman LE, Fleysher L, Steenwijk MD, Koeleman JA, de Snoo T-P, Barkhof F, et al. Ultra-high field MTR and qR2* differentiates subpial cortical lesions from normal-appearing gray matter in multiple sclerosis. *Mult. Scler*. 2016; 22: 1306–1314.
- Kalincik T, Cutter G, Spelman T, Jokubaitis V, Havrdova E, Horakova D, et al. Defining reliable disability outcomes in multiple sclerosis. *Brain*. 2015; 138: 3287–3298.
- Kapoor R, Furby J, Hayton T, Smith KJ, Altmann DR, Brenner R, et al. Lamotrigine for neuroprotection in secondary progressive multiple sclerosis: a randomised, double-blind, placebo-controlled,

parallel-group trial. *Lancet Neurol.* 2010; 9: 681–688.

Kappos L, Bar-Or A, Cree BAC, Fox RJ, Giovannoni G, Gold R, et al. Siponimod versus placebo in secondary progressive multiple sclerosis (EXPAND): a double-blind, randomised, phase 3 study. *Lancet* 2018

Kawachi I, Lassmann H. Neurodegeneration in multiple sclerosis and neuromyelitis optica. *J. Neurol. Neurosurg. Psychiatry* 2017; 88: 137–145.

Khaleeli Z, Cercignani M, Audoin B, Ciccarelli O, Miller DH, Thompson AJ. Localized grey matter damage in early primary progressive multiple sclerosis contributes to disability. *Neuroimage* 2007; 37: 253–261.

Khaleeli Z, Ciccarelli O, Manfredonia F, Barkhof F, Brochet B, Cercignani M, et al. Predicting progression in primary progressive multiple sclerosis: a 10-year multicenter study. *Ann Neurol.* 2008; 63: 790–793.

Khaleeli Z, Ciccarelli O, Mizskiel K, Altmann D, Miller D, Thompson A. Lesion enhancement diminishes with time in primary progressive multiple sclerosis. *Mult Scler* 2010; 16: 317–324.

Khaleeli Z, Sastre-Garriga J, Ciccarelli O, Miller D, Thompson A. Magnetisation transfer ratio in the normal appearing white matter predicts progression of disability over 1 year in early primary progressive multiple sclerosis. *J Neurol Neurosurg Psychiatry* 2007; 78: 1076–1082.

Kilsdonk ID, Jonkman LE, Klaver R, Van Veluw SJ, Zwanenburg JJM, Kuijjer JPA, et al. Increased cortical grey matter lesion detection in multiple sclerosis with 7 T MRI: A post-mortem verification study. *Brain.* 2016; 139: 1472–1481.

Kinzel S, Weber MS. B Cell-Directed Therapeutics in Multiple Sclerosis: Rationale and Clinical Evidence. *CNS Drugs* 2016; 30: 1137–1148.

Kuhlmann T, Ludwin S, Prat A, Antel J, Brück W, Lassmann H. An updated histological classification system for multiple sclerosis lesions. *Acta Neuropathol.* 2017; 133: 13–24.

Lassmann H. Targets of therapy in progressive MS. *Mult. Scler.* 2017; 23: 1593–1599.

Lassmann H. Multiple sclerosis pathology. *Cold Spring Harb. Perspect. Med.* 2018; 8: 1–16.

Lassmann H, Raine CS, Antel J, Prineas JW. Immunopathology of multiple sclerosis: Report on an international meeting held at the Institute of Neurology of the University of Vienna. *J. Neuroimmunol.* 1998; 86: 213–217.

Lee JS, Ahn S-H, Lee DS, Oh SH, Kim CS, Jeong JM, et al. Voxel-based statistical analysis of cerebral glucose metabolism in the rat cortical deafness model by 3D reconstruction of brain from autoradiographic images. *Eur. J. Nucl. Med. Mol. Imaging* 2005; 32: 696–701.

Lee PW, Xin MK, Pei W, Yang Y, Lovett-Racke AE. IL-3 Is a Marker of Encephalitogenic T Cells, but Not Essential for CNS Autoimmunity. *Front. Immunol.* 2018; 9: 1–7.

Legroux L, Arbour N. Multiple Sclerosis and T Lymphocytes: An Entangled Story. *J. Neuroimmune Pharmacol.* 2015; 10: 528–546.

Li S, Clements R, Sulak M, Gregory R, Freeman E, McDonough J. Decreased NAA in gray matter is correlated with decreased availability of acetate in white matter in postmortem multiple sclerosis cortex. *Neurochem Res.* 2013; 38: 2385–2396.

Liddel SA, Guttenplan KA, Clarke LE, Bennett FC, Bohlen CJ, Schirmer L, et al. Neurotoxic reactive astrocytes are induced by activated microglia. *Nature* 2017; 541: 481–487.

Lin C-C, Edelson BT. New Insights into the Role of IL-1 β in Experimental Autoimmune Encephalomyelitis and Multiple Sclerosis. *J. Immunol.* 2017; 198: 4553–4560.

Lublin FD, Reingold SC, Cohen JA, Cutter GR, Thompson AJ, Wolinsky JS, et al. Defining the clinical course of multiple sclerosis. *Am. Acad. Neurol.* 2014; 83: 278–286.

Lublin FD, Reingold SC, Cohen JA, Cutter GR, Sørensen PS, Thompson AJ, et al. Defining the clinical course of multiple sclerosis : The 2013 revisions. *Neurology* 2014; 83: 278–286.

Lucchinetti CF, Brück W, Parisi JE, Scheithauer BW, Rodriguez M, Lassmann H. Heterogeneity of Multiple Sclerosis Lesions: Implications for the Pathogenesis of Demyelination. *Ann Neurol.* 2000; 47: 707–717.

Magliozzi R, Howell O, Nicholas R, Cruciani C, Castellaro M, Romualdi C, et al. Inflammatory intrathecal profiles and cortical damage in multiple sclerosis. *Ann Neurol*. 2018; 83: 739–755.

Magliozzi R, Howell O, Vora A, Serafini B, Nicholas R, Puopolo M, et al. Meningeal B-cell follicles in secondary progressive multiple sclerosis associate with early onset of disease and severe cortical pathology. *Brain*. 2007; 130: 1089–1104.

Magliozzi R, Howell OW, Reeves C, Roncaroli F, Nicholas R, Serafini B, et al. A Gradient of neuronal loss and meningeal inflammation in multiple sclerosis. *Ann Neurol*. 2010

Magliozzi R, Reynolds R, Calabrese M. MRI of cortical lesions and its use in studying their role in MS pathogenesis and disease course. *Brain Pathol*. 2018

Magliozzi R, Serafini B, Rosicarelli B, Chiappetta G, Veroni C, Reynolds R, et al. B-cell enrichment and Epstein-Barr virus infection in inflammatory cortical lesions in secondary progressive multiple sclerosis. *J. Neuropathol. Exp. Neurol*. 2013

Mallik S, Samson RS, Wheeler-Kingshott CAM, Miller DH. Imaging outcomes for trials of remyelination in multiple sclerosis. *J Neurol Neurosurg Psychiatry*. 2014; 85: 1396–1404.

Martinez Sosa S, Smith KJ. Understanding a role for hypoxia in lesion formation and location in the deep and periventricular white matter in small vessel disease and multiple sclerosis. *Clin. Sci*. 2017; 131: 2503–2524.

Metz I, Weigand SD, Popescu BFG, Frischer JM, Parisi JE, Guo Y, et al. Pathologic heterogeneity persists in early active multiple sclerosis lesions. *Ann Neurol*. 2014; 75: 728–738.

Miller D, Leary S. Primary-progressive multiple sclerosis. *Lancet Neurol*. 2007; 6: 903–912.

Moccia M, Capacchione A, Lanzillo R, Carbone F, Micillo T, Perna F, et al. Coenzyme Q10 supplementation reduces peripheral oxidative stress and inflammation in Interferon-Beta1a treated multiple sclerosis. *Ther. Adv. Neurol. Disord*. 2018

Moccia M, Ciccarelli O. Molecular and Metabolic Imaging in Multiple Sclerosis. *Neuroimaging Clin. N. Am*. 2017; 27: 343–356.

Moccia M, Ciccarelli O. Molecular and Metabolic Imaging in Multiple Sclerosis. *Neuroimaging Clin. N. Am.* 2017; 27: 343–356.

Moccia M, Lanzillo R, Costabile T, Russo C, Carotenuto A, Sasso G, et al. Uric acid in relapsing–remitting multiple sclerosis: a 2-year longitudinal study. *J Neurol.* 2015; 262: 961–967.

Moccia M, Lanzillo R, Costabile T, Russo C, Carotenuto A, Sasso G, et al. Uric acid in relapsing–remitting multiple sclerosis: a 2-year longitudinal study. *J Neurol.* 2015; 262: 961–967.

Moccia M, Lanzillo R, Palladino R, Maniscalco GT, De Rosa A, Russo C, et al. The Framingham cardiovascular risk score in multiple sclerosis. *Eur J Neurol.* 2015; 22

Moccia M, Lanzillo R, Palladino R, Russo C, Carotenuto A, Massarelli M, et al. Uric acid : a potential biomarker of multiple sclerosis and of its disability. *Clinical Chem Lab Med.* 2015; 53: 753–759.

Moccia M, Picillo M, Erro R, Vitale C, Longo K, Amboni M, et al. Presence and progression of non-motor symptoms in relation to uric acid in de novo Parkinson ' s disease. *Eur J Neurol.* 2015; 22: 93–98.

Moccia M, Quarantelli M, Lanzillo R, Coccozza S, Carotenuto A, Carotenuto B, et al. Grey:white matter ratio at diagnosis and the risk of 10-year multiple sclerosis progression. *Eur J Neurol.* 2017; 24

Moccia M, de Stefano N, Barkhof F. Imaging outcome measures for progressive multiple sclerosis trials. *Mult. Scler.* 2017; 23

Modat M, Cash DM, Daga P, Winston GP, Duncan JS, Ourselin S. Global image registration using a symmetric block-matching approach. *J. Med. Imaging* 2014; 1: 024003.

Modat M, Ridgway GR, Taylor ZA, Lehmann M, Barnes J, Hawkes DJ, et al. Fast free-form deformation using graphics processing units. *Comput. Methods Programs Biomed.* 2010; 98: 278–284.

Moll NM, Rietsch AM, Thomas S, Ransohoff AJ, Lee JC, Fox R, et al. Multiple sclerosis normal-appearing white matter: Pathology-imaging correlations. *Ann Neurol.* 2011; 70: 764–773.

Molnarfi N, Benkhoucha M, Bjarnadóttir K, Juillard C, Lalive PH. Interferon- β Induces Hepatocyte

- Growth Factor in Monocytes of Multiple Sclerosis Patients. *PLoS One*. 2012; 7: e49882.
- Montalban X, Hauser SL, Kappos L, Arnold DL, Bar-Or A, Comi G, et al. Ocrelizumab versus Placebo in Primary Progressive Multiple Sclerosis. *N. Engl. J. Med.* 2017; 376: 209–220.
- Mottershead JP, Schmierer K, Clemence M, Thornton JS, Scaravilli F, Barker GJ, et al. High field MRI correlates of myelin content and axonal density in multiple sclerosis: A post-mortem study of the spinal cord. *J Neurol.* 2003; 250: 1293–1301.
- National Multiple Sclerosis Society. MS Symptoms. National Multiple Sclerosis Society Website. MS Symptoms 2016
- Nicol B, Salou M, Laplaud DA, Wekerle H. The autoimmune concept of multiple sclerosis. *Press. Medica* 2015; 44: e103–e112.
- Ntranos A, Lublin F. Diagnostic Criteria, Classification and Treatment Goals in Multiple Sclerosis: The Chronicles of Time and Space. *Curr. Neurol. Neurosci. Rep.* 2016; 16: 90.
- O'Brien A, Gaudino-Goering E, Shawaryn M, Komaroff E, Moore NB, DeLuca J. Relationship of the Multiple Sclerosis Neuropsychological Questionnaire (MSNQ) to functional, emotional, and neuropsychological outcomes. *Arch. Clin. Neuropsychol.* 2007; 22: 933–948.
- Ontaneda D, Fox RJ. Imaging as an Outcome Measure in Multiple Sclerosis. *Neurotherapeutics* 2017; 14: 24–34.
- Otsu N. A Threshold Selection Method from Gray-Level Histograms. *IEEE Trans. Syst. Man Cybern.* 1979; 20: 62–66.
- Patodia S, Somani A, O'Hare M, Venkateswaran R, Liu J, Michalak Z, et al. The ventrolateral medulla and medullary raphe in sudden unexpected death in epilepsy. *Brain.* 2018
- Pichat J, Iglesias JE, Yousry T, Ourselin S, Modat M. A Survey of Methods for 3D Histology Reconstruction. *Med. Image Anal.* 2018; 46: 73–105.
- Pittaluga A. CCL5-glutamate cross-talk in astrocyte-neuron communication in multiple sclerosis. *Front. Immunol.* 2017; 8: 1079.

Plemel JR, Juzwik CA, Benson CA, Monks M, Harris C, Ploughman M. Over-the-counter anti-oxidant therapies for use in multiple sclerosis: A systematic review. *Mult. Scler.* 2015; 21: 1485–1495.

Polman CH, Reingold SC, Banwell B, Clanet M, Cohen J a., Filippi M, et al. Diagnostic criteria for multiple sclerosis: 2010 Revisions to the McDonald criteria. *Ann Neurol.* 2011; 69: 292–302.

Ponath G, Park C, Pitt D. The Role of Astrocytes in Multiple Sclerosis. *Front. Immunol.* 2018; 9: 217.

Popescu V, Agosta F, Hulst HE, Ingrid C, Knol DL, Sormani MP, et al. Brain atrophy and lesion load predict long-term disability in multiple sclerosis. *J. Neurol. Neurosurg. Psychiatry* 2013; 84: 1082–1091.

Prins M, Schul E, Geurts J, van der Valk P, Drukarch B, van Dam AM. Pathological differences between white and grey matter multiple sclerosis lesions. *Ann N Y Acad Sci.* 2015; 1351: 99–113.

Ranjeva J-P, Audoin B, Van Au Duong M, Ibarrola D, Confort-Gouny S, Malikova I, et al. Local Tissue Damage Assessed with Statistical Mapping Analysis of Brain Magnetization Transfer Ratio: Relationship with Functional Status of Patients in the Earliest Stage of Multiple Sclerosis. *Am. J. Neuroradiol.* 2005; 26: 119–127.

Reich DS, Lucchinetti CF, Calabresi PA. Multiple Sclerosis. *N. Engl. J. Med.* 2018; 378: 169–180.

Rocca MA, Absinta M, Filippi M. The role of advanced magnetic resonance imaging techniques in primary progressive MS. *J Neurol.* 2012; 259: 611–621.

Rodríguez-Antigüedad Zarranz A, Mendibe Bilbao M, Llarena González C, Audicana C. Mortality and cause of death in multiple sclerosis: Findings from a prospective population-based cohort in bizkaia, basque country, Spain. *Neuroepidemiology* 2014; 42: 219–225.

Roman I, Figys J, Steurs G, Zizi M. In vitro interactions between the two mitochondrial membrane proteins VDAC and cytochrome c oxidase. *Biochemistry* 2005; 44: 13192–13201.

Romme Christensen J, Ratzner R, Bornsen L, Lyksborg M, Garde E, Dyrby TB, et al. Natalizumab in progressive MS. *Neurology* 2014; 82: 1499–1507.

Rossi S, Studer V, Motta C, Polidoro S, Perugini J, Macchiarulo G, et al. Neuroinflammation drives

- anxiety and depression in relapsing-remitting multiple sclerosis. *Neurology* 2017; 89: 1338–1347.
- Rovaris M, Judica E, Sastre-Garriga J, Rovira A, Sormani M, Benedetti B, et al. Large-scale, multicentre, quantitative MRI study of brain and cord damage in primary progressive multiple sclerosis. *Mult. Scler.* 2008; 14: 455–464.
- Ruggieri S, Tortorella C, Gasperini C. Anti lingo 1 (opicinumab) a new monoclonal antibody tested in relapsing remitting multiple sclerosis. *Expert Rev. Neurother.* 2017
- Sanders V, Conrad AJ, Tourtellotte WW. On classification of post-mortem multiple sclerosis plaques for neuroscientists. *J. Neuroimmunol.* 1993; 46: 207–216.
- Sanoobar M, Dehghan P, Khalil M, Azimi A, Seifar F. Coenzyme Q10 as a treatment for fatigue and depression in multiple sclerosis patients: A double blind randomized clinical trial. *Nutr. Neurosci.* 2016; 19: 138–143.
- Sanoobar M, Dehghan P, Khalili M, Azimi A, Seifar F. Coenzyme Q10 as a treatment for fatigue and depression in multiple sclerosis patients: A double blind randomized clinical trial. *Nutr. Neurosci.* 2016; 19: 138–143.
- Sanoobar M, Eghtesadi S, Azimi A, Khalili M, Jazayeri S, Gohari MR. Coenzyme Q10 supplementation reduces oxidative stress and increases antioxidant enzyme activity in patients with coronary artery disease. *Int J Neurosci.* 2013; 123: 776–782.
- Sanoobar M, Eghtesadi S, Azimi A, Khalili M, Khodadadi B, Jazayeri S, et al. Coenzyme Q10 supplementation ameliorates inflammatory markers in patients with multiple sclerosis: a double blind, placebo, controlled randomized clinical trial. *Nutr. Neurosci.* 2015; 18: 169–176.
- Scalfari A, Romualdi C, Nicholas RS, Mattosio M, Magliozzi R, Morra A, et al. The cortical damage, early relapses, and onset of the progressive phase in multiple sclerosis. *Neurology* 2018
- Schmierer K, Parkes HG, So P-W, An SF, Brandner S, Ordidge RJ, et al. High field (9.4 Tesla) magnetic resonance imaging of cortical grey matter lesions in multiple sclerosis. *Brain.* 2010; 133: 858–867.
- Schmierer K, Scaravilli F, Altmann DR, Barker GJ, Miller DH. Magnetization transfer ratio and myelin

in postmortem multiple sclerosis brain. *Ann Neurol.* 2004; 56: 407–415.

Schmierer K, Thavarajah JR, An SF, Brandner S, Miller DH, Tozer DJ. Effects of formalin fixation on magnetic resonance indices in multiple sclerosis cortical gray matter. *J. Magn. Reson. Imaging* 2010; 32: 1054–1060.

Schmierer K, Tozer DJ, Scaravilli F, Altmann DR, Barker GJ, Tofts PS, et al. Quantitative magnetization transfer imaging in postmortem multiple sclerosis brain. *J. Magn. Reson. Imaging* 2007; 26: 41–51.

Schmierer K, Wheeler-Kingshott CAM, Tozer DJ, Boulby PA, Parkes HG, Yousry TA, et al. Quantitative magnetic resonance of postmortem multiple sclerosis brain before and after fixation. *Magn. Reson. Med.* 2008; 59: 268–277.

Schwartzbach CJ, Grove RA, Brown R, Tompson D, Then Bergh F, Arnold DL. Lesion remyelinating activity of GSK239512 versus placebo in patients with relapsing-remitting multiple sclerosis: a randomised, single-blind, phase II study. *J Neurol.* 2017; 264: 304–315.

Sedgwick P. What is a crossover trial? *BMJ* 2014; 348: 9–10.

Shoshan-Barmatz V, De Pinto V, Zweckstetter M, Raviv Z, Keinan N, Arbel N. VDAC, a multi-functional mitochondrial protein regulating cell life and death. *Mol. Aspects Med.* 2010; 31: 227–285.

Sormani MP, Arnold DL, De Stefano N. Treatment effect on brain atrophy correlates with treatment effect on disability in multiple sclerosis. *Ann Neurol.* 2014; 75: 43–49.

Sormani MP, Bruzzi P. MRI lesions as a surrogate for relapses in multiple sclerosis: A meta-analysis of randomised trials. *Lancet Neurol.* 2013; 12: 669–676.

Spindler M, Flint Beal M, Henchcliffe C. Coenzyme Q10 effects in neurodegenerative disease. *Neuropsychiatr. Dis. Treat.* 2009; 5: 597–610.

Stampanoni Bassi M, Iezzi E, Landi D, Monteleone F, Gilio L, Simonelli I, et al. Delayed treatment of MS is associated with high CSF levels of IL-6 and IL-8 and worse future disease course. *J Neurol.* 2018

Stangel M, Kuhlmann T, Matthews PM, Kilpatrick TJ. Achievements and obstacles of remyelinating therapies in multiple sclerosis. *Nat. Rev. Neurol.* 2017; 13: 742–754.

Steri M, Orrù V, Idda M, Pitzalis M, Pala M, Zara I, et al. Overexpression of the Cytokine BAFF and Autoimmunity Risk. *N. Engl. J. Med.* 2017; 376: 1615–1626.

Tavakolpour S. Interleukin 7 receptor polymorphisms and the risk of multiple sclerosis: A meta-analysis. *Mult. Scler. Relat. Disord.* 2016; 8: 66–73.

Thompson AJ, Baranzini SE, Geurts J, Hemmer B, Ciccarelli O. Multiple sclerosis. *Lancet* 2018; 391: 1622–1636.

Trapp BD, Vignos M, Dudman J, Chang A, Fisher E, Staugaitis SM, et al. Cortical neuronal densities and cerebral white matter demyelination in multiple sclerosis: a retrospective study. *Lancet Neurol.* 2018; 17: 870–884.

Tur C. Fatigue Management in Multiple Sclerosis. *Curr. Treat. Options Neurol.* 2016; 18: 26.

Tur C, Moccia M, Barkhof F, Chataway J, Sastre-Garriga J, Thompson AJ, et al. Assessing treatment outcomes in multiple sclerosis trials and in the clinical setting. *Nat. Rev. Neurol.* 2018; 14: 75–93.

Van Der Valk P, De Groot CJA. Staging of multiple sclerosis (MS) lesions: Pathology of the time frame of MS. *Neuropathol. Appl. Neurobiol.* 2000; 26: 2–10.

Vavasour IM, Laule C, Li DKB, Traboulsee AL, MacKay AL. Is the magnetization transfer ratio a marker for myelin in multiple sclerosis? *J. Magn. Reson. Imaging* 2011; 33: 713–718.

Wattjes M, Rovira A, Miller D, Yousry T, Sormani M, de Stefano N, et al. Evidence-based guidelines: MAGNIMS consensus guidelines on the use of MRI in multiple sclerosis—establishing disease prognosis and monitoring patients. *Nat Rev Neurol* 2015; 11: 597–606.

Yang R, Dunn JF. Multiple sclerosis disease progression: Contributions from a hypoxia–inflammation cycle. *Mult. Scler.* 2018

Zoghi S, Amirghofran Z, Nikseresht A, Ashjazadeh N, Kamali-Sarvestani E, Rezaei N. Cytokine secretion pattern in treatment of lymphocytes of multiple sclerosis patients with fumaric acid esters. *Immunol. Invest.* 2011; 40: 581–596.